RSC Advances

ROYAL SOCIETY OF CHEMISTRY

www.rsc.org/advances

Journal Name

RSCPublishing

ARTICLE

Advances in nanomaterial based approaches for enhanced fluoride and nitrate removal from contaminated water

S. P. Suriyaraj[a] and R. Selvakumar[a,*]

Cite this: DOI: 10.1039/x0xx00000x

Received 00th January 2013,
Accepted 00th January 2013

DOI: 10.1039/x0xx00000x

www.rsc.org/

Fluoride and nitrate contamination in drinking water sources have been a major problem in many countries. The long term health hazards and increasing levels of fluoride and nitrate in drinking water through natural and anthropogenic sources have been challenging and warrants the need for advanced technologies for abating these contaminants. Various technologies have been reported so far for fluoride and nitrate removal from drinking water. Recent advances in nanotechnology and nanomaterial synthesis have showed significant impact on fluoride and nitrate removal when compared to other conventional adsorbents and process. The present review discusses the recent advances in nanotechnology and nanomaterials synthesis, modification in process parameters and use for composite nanomaterials for enhanced removal of fluoride and nitrate from contaminated water.

1. Introduction

Water pollution is a major problem in developing countries; especially the regions where people depend on groundwater for drinking.[1]Nearly forty percent of the world's population is already facing water shortage; the cost of water infrastructure has also increased dramatically. The quality of water in rivers and underground has deteriorated, due to pollution by waste and contaminants from cities, industry and agriculture.[2] Natural water bodies have impurities from various sources. The most common contaminants are microorganisms, suspended particles, colloidal materials, pesticides and various dissolved metallic and non-metallic substances.[3,4] Among these compounds, anionic pollutants like fluoride and nitrate contamination in groundwater has been recognized as one of the serious problem worldwide.[5-7] Various diseases and harmful effects caused by drinking, fluoride and nitrate contaminated water have been a great anxious to our human society.

An excessive fluoride intake leads to loss of calcium from the tooth matrix, causing cavity formation, and ultimately leads to dental fluorosis followed by skeletal fluorosis after prolonged exposure.[8-9] Fluoride has been implicated in a number of adverse outcomes related to fertility and pregnancy.[10] Diseases like Alzheimer, bladder cancer, thyroid disorder, gastrointestinal bleeding and otosclerosis, can attack human body on excessive intake of fluoride.[11-13] Similarly excessive nitrate intake leads to gastric cancer, goitre, birth malformations, hypertension and methemoglobinemia.[14,15] Prolonged intakes of high levels of nitrate are linked to gastric problems due to the formation of nitrosamines. N-nitrosamine compounds have been shown to cause cancer in test animals. Studies on people exposed to high levels of nitrate or nitrite have not provided convincing evidence of an increased risk of cancer.[14-17] Other health effects following fetal exposure to elevated levels of nitrates in drinking water, included intrauterine growth retardation, increased incidence of Sudden Infant Death Syndrome (SIDS), cardiac defects, and increased risk of nervous system defects.[18-20] Few studies have reported other health effects that are possibly associated with nitrate exposure in children, including increased incidence of childhood diabetes, recurrent diarrhea and respiratory tract infections.[14,19]

Due to these clinical manifestations caused by drinking fluoride and nitrate contaminated water, World Health Organization (WHO) has recommended 1.5 mg/L and 45 mg/L as the maximum contaminant level (MCL) in drinking water for fluoride and nitrate respectively.[21] Hence, it is an important issue to supply water with safe F^- and NO_3^- levels. Various methods like chemical precipitation, electrocoagulation, reverse osmosis and electrodialysis have been reported to remove fluoride and nitrate from drinking water.[22-26] Despite of unique advantages in these technologies, the cost factor, poor regeneration, interference of other ions, customary replacement of sacrificial electrodes, consumption of electric power, membrane fouling, requirement of experienced operators and poor water recoveries always remains a problem and create limited social acceptance of these technologies.[23-25] Scientific evidences recommend adsorption and photocatalysis as most

efficient and cost effective method to remove fluoride and nitrate when compared to other methods.[27,15]

Various type of materials like activated carbon, activated alumina, zeolites, hematite, schwertmannite various geo-materials, bio-sorbents, industrial products, polymer resins/fibers/membranes, organics, different metal oxides, composites, and more recently variety of nanomaterials have been studied for the removal of fluoride and nitrate from aqueous solution.[23-33] Among them, the selective nano based materials and composites have good potential for removal of fluoride and nitrate from aquatic environments. The role of nanoscience and its technology have opened new avenues and lay a hand on many useful and powerful applications in the field of environmental safety such as water purification.[34-37] Nanomaterials offer the possibility for an efficient removal of various pollutants like fluorides, nitrates and various toxic ions from drinking water.[15,27-28] It has been found that the unique properties of various metal and non metal nanomaterials can be used to develop high capacity and selective sorbents for metal ions removal from drinking water.[38-40] Hence, this review focuses on a conceptual overview of the recent trends, principles, application of advanced nanomaterials for removal of F^- and NO_3^- from aqueous solution.

2. Advanced nanomaterials for fluoride removal

2.1. Metal oxide nanomaterials

In past ten years, many researchers have devoted their attention to develop low cost and effective adsorbent nanomaterials for the removal of fluorides from aqueous solution and contaminated water. The fluoride adsorption was determined by various factors like effect of contact time, adsorbent dosage, adsorbate concentration, pH and temperature.[29,30] Various inorganic nanomaterials play a vital role in the removal of fluorides from aqueous solution. Among them iron, alumina, titania, magnesia, silica, zirconium, cerium and calcium based metal oxide nanomaterials/composites play an important role in the defluorination process.[27-30] These types of oxide nanomaterials are rich in surface functional groups, which is highly stable in adsorbing fluorides from aqueous solution. Increased surface area of the metal oxide nanoparticles highly favours fluoride adsorption.[41-45] High adsorption capacity, non-toxic nature, limited solubility in water and its desorption potential makes metal oxides a material of choice.[41-45] These metal oxides have been modified using various methods for preparing hybrid/core shell nanomaterials that can increase further fluoride removal. The porous nature of the adsorbent also plays a major role in the fluoride adsorption. Highly mesoporous CeO_2/Al_2O_3 and CeO_2/Mg–Fe metal oxides, having less than 50 nm porosity was prepared by Zhang *et al.* using non-thermal plasma modification method.[46,47] The mesoporous metal oxide nanomaterials provided high fluoride adsorption efficiency of 37–60 mg/g which might be due to the increased adsorption sites, large surface area and its mesoporous structure. The columbic or ligand exchange type of fluoride adsorption may also be one of the important mechanisms for fluoride adsorption. Biswas et al. (2010) synthesised spherical hydrous iron (III) - chromium (III) bimetal mixed oxide spherical nano particles of 40–55 nm using co-precipitation method. These hybrid bimetal nanoparticles had 16.34 mg/g fluoride adsorption capacity and required a optimum contact time of 30 min.The adsorption was attributed towards rapid boundary layer diffusion on to the surface of the bimetal mixed oxide nanoparticle.[48] The adsorption is due to rapid boundary layer diffusion of the dissolved fluoride onto the surface of the mixed metal oxide nanoparticle. Mn–Ce oxide adsorbent of about 4.5 nm crystals prepared by Deng *et al.* [49] via co-precipitation method showed high fluoride adsorption efficiency of 79.5 mg/g within one hour. According to the author, the surface hydroxyl group density caused by the entry of Mn species into the CeO_2 lattices on the Mn–Ce adsorbent is mainly responsible for its high adsorption capacity towards fluoride. Further the anion exchange and electrostatic interaction were involved in the sorption of fluoride on the Mn–Ce oxide adsorbent. Similarly, the hydrous Ce(IV)–Zr(IV) oxide nanoparticles of about 60–70 nm, prepared by simple chemical precipitation by Ghosh *et al.* [50] showed fluoride adsorption capacity of ~19.5 mg/g. The mechanism proposed is similar with other previous reports for fluoride adsorption over metal oxide surface. CTAB mediated Mg-doped nano Fe_2O_3 of particle size ranging from 40–200 nm was synthesized using precipitation technique by Mohapatra *et al.* [51] showed fluoride adsorption efficiency of 75.2 mg/g. The thermodynamic studies of the material by the author revels that, the fluoride adsorption on Mg-doped nano hematite particles was thermodynamically favourable at low temperatures and was exothermic in nature.

Porous and hollow MgO microspheres with a high surface area of 130 m^2/g were prepared by Li et al. [52] using precursor calcination method. These microspheres composed of MgO nanoparticles on to its surface gave high fluoride adsorption efficiency of >120 mg/g. The reaction between MgO and water molecules resulted in the formation of magnesium hydroxides ($Mg(OH)_2$)which then reacted with fluoride ion to form $Mg(OH)_{2-x}F_x$, yielding excellent defluoridation effect.

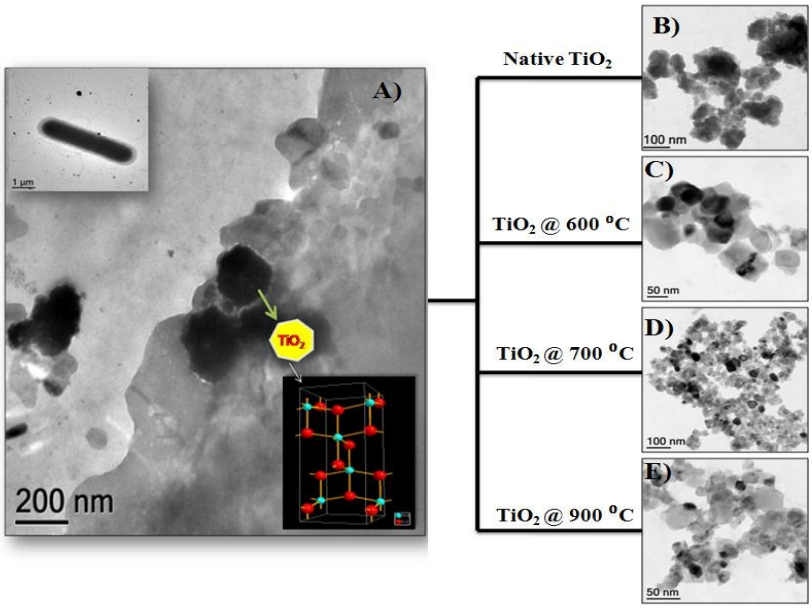

Fig.1 A) Biosynthesis of TiO_2nanoparticles using microbial approach,A insert)Bacillus NARW11 species used for TiO_2 synthesis, B) native TiO_2 without calcination, C) anatase pure TiO_2 calcined at 600ºC, D) anatase mix rutile TiO_2 calcined at 700ºC, E) rutile pure TiO_2 calcined at 900ºC. (Adapted from ref 27 with permission from Elsevier)

The adsorption of fluoride on Ti–Al binary metal oxide supported beads were studied by Thakre et al.[53] by varying initial fluoride concentration and keeping other parameters constant such as; the optimum dose of 4 g/L, temperature (30 ºC) and contact time of 24 h. It was observed that with increase in initial adsorbate concentration, the percentage removal decreased. Native TiO_2, Ti-Ce, and Ti-La hybrid oxide materials for the fluoride adsorption were reported by Li et al.[54] The Ti-Ce and Ti-La hybrid adsorbents obtained by the hydrolysis-precipitation method had much higher sorption capacity for fluoride than the TiO_2 adsorbent prepared through hydrolysis. The adsorption capacities of fluoride on the Ti-Ce and Ti-La adsorbents with respect to fluoride were 9.6 and 15.1 mg/g respectively.

Recently, adsorption of fluoride using bio-titania nanoparticles synthesized using microbial approach was reported by our group (Suriyaraj et al., [27]). Metal resistant *Bacillus* NARW 11 species was used for the synthesis of native TiO_2 nanoparticles (Fig. 1(A) and insert). The native microbially synthesized bio-titania nanoparticles showed anatase crystalline nature (Fig. 1(B). The native TiO_2 nanoparticle were subjected to calcination at various temperatures and different crystalline phase structures like pure anatase Fig. 1(C), anatase mix rutile Fig. 1(D) and pure rutile Fig. 1(E) were achieved. Among the various phases of TiO_2 nanoparticles, anatase phase showed highest fluoride adsorption capacity (0.85 mg/g). The nanoparticle also showed good desorption potential indicating that the adsorbents can be reused. These nanoparticles, synthesis using eco-friendly and green approach can be an alternative to caustic chemical synthesis protocols.

Hence the fundamental mechanism of fluoride adsorption using various nanomaterials is based on the electrostatic attraction or ligand-exchange reaction between fluoride and hydroxyl ions, which in turn takes place according to the pH of the medium. At acidic pH, positively charged surface sites are developed which attract the negatively charged fluoride ions by electrostatic attraction resulting in the enhanced fluoride removal in acidic pH. At neutral pH, fluoride adsorption can be due to the ligand-exchange reaction between fluoride and hydroxyl ions. In the presence of other ions like nitrate, sulphate and phosphate etc. in water, the fluoride adsorption may takes place due to its smaller ionic radii (0.133 nm). Hence it can easily accommodated in nanomaterials especially in porous structures. Moreover, the process may be a chemical adsorption process involving valence forces through sharing or exchange of electrons between nanomaterials and fluoride ion. In case of mesoporous structured nanoadsorbents, the adsorption of fluoride ions mostly takes place by intra particle diffusion mechanism.[27,28,55]

2.2. Magnetic nanomaterials

Some of the metal oxide adsorbents with magnetic property are highly efficient in fluoride adsorption as well as the removal of adsorbent after the reaction. Even though the nanocomposite adsorbents show good adsorbent potential, the retract of adsorbent from aqueous solution after completion of reaction is a main problem till now and even the nanoparticles can be easily leached into the water system.[29,30] In order to overcome this problem, various metal oxides prepared with magnetic property provides a promising way to perform solid–liquid separation of the nano-adsorbent and water. Various iron oxide

based nanomaterials/composites play a significant role under this category.

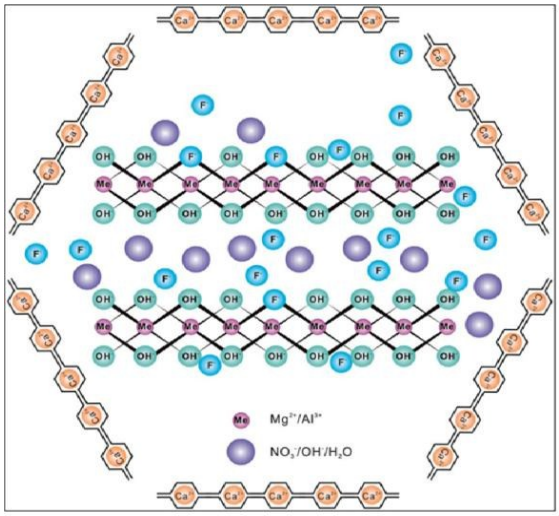

Fig. 2 Complex adsorption process by LDH-n-MABs on fluoride removal. Reprinted from ref 63 with permission from the Royal Society of Chemistry.

Sulfate-doped Fe_3O_4/Al_2O_3 prepared by chemical co-precipitation method showed maximum fluoride adsorption of about 70.4 mg/g at pH 7.0 (Chai *et al.*[56]). The results revealed that the sulfate-fluoride displacement and the decreased sulfur content on the nanomaterial surface contributing to anion exchange process was an important mechanism for fluoride adsorption by the sulfate doped Fe_3O_4/Al_2O_3nanoparticles. The Fe–Ti bimetallic oxide nano-adsorbents synthesized by Chen *et al.* [57] and Zhang *et al.* [58] using co-precipitation method showed better adsorption capacity which was much superior than the pure Fe oxide or Ti oxide adsorbents. The fluoride adsorption may be due to the interaction between Fe and Ti in Fe–O–Ti bonds on the nanomaterials surface and OH groups which provided the active sites and formation of Fe–O–Ti–F bonds during the adsorption process. Zirconium (IV)-metalloporphyrin grafted Fe_3O_4 nanoparticle having average size of 56 nm was synthesized by co-precipitation method.[59] The material had the efficiency to remove 92.0 ±1.7% of fluoride for the initial adsorbate concentration of 10 mg/L within the contact time of 20 min. Experiments reported that the functionalization of zirconium (IV) - metalloporphyrin showed good efficiency in fluoride adsorption with high specificity and selectivity. Similarly the magnesium oxide (MgO)-coated magnetite (Fe_3O_4) nanoparticle with magnetic property was synthesized by Minju *et al.*[60] using modified sol-gel method for analyzing the fluoride scavenging potential. The adsorption capacity was found to be 10.96 mg/g. The adsorbent showed an excellent fluoride scavenging potential for the initial fluoride concentration up to 10 mg/L. The magnetic nanosized adsorbent using hydrous aluminum oxide embedded with Fe_3O_4 nanoparticle was prepared by Zhao *et al.*[61] to study fluoride removal from aqueous solution. The maximum adsorption capacity was found to be 88.48 mg/g under neutral pH at room temperature. A distinct advantage of this defluoridation procedure is that the adsorbents can readily be isolated from sample solutions by the application of an external magnetic field. According to the author, the material has three attractive properties like high adsorption capacity, rapid defluoridation treatment and easy preparation, which can meet the need of practical application for treatment of large volume high-fluoride contaminated water. Polypyrrole (PPy)/Fe_3O_4 magnetic nanocomposite adsorbent was prepared by Bhaumika *et al.*[62] via in-situ polymerization. The fluoride adsorption capacity of the nanocomposites was found to be in the range of 17.6–22.3 mg/g. Another easy and effective magnetic based Mg–Al-LDH nanoflake impregnated magnetic alginate beads (LDH-n-MABs) prepared by Gao *et al.*[63] showed increased adsorption efficiency of about 32.4 mg/g. The nanomaterial had many potential advantages like the low leaching due to immobilisation into alginate beads, high magnetic sensitivity, biodegradability etc. The author explained that the complex adsorption process is responsible for the higher fluoride adsorption efficiency of the LDH-n-MABs (**Fig. 2**). Similarly the Fe_3O_4 nanoparticles in a network of Zr(IV) complexed poly(acrylamide) (Zr–PAM) prepared by encapsulation method is one of the best fluoride ion selective magnetic sorbent.[64] The material has high adsorption efficiency of 124.5 mg/g. The pictorial representation of the magnetic separation of nanoparticles after the completion of fluoride adsorption is shown in the **Fig 3**. Hence magnetic separation has been a promising method for solid–liquid phase separation technique with various advantages like high absorption capacity, high speed, accuracy, simplicity and efficient solid–liquid separation when compared to the conventional separation methods.[56-58]

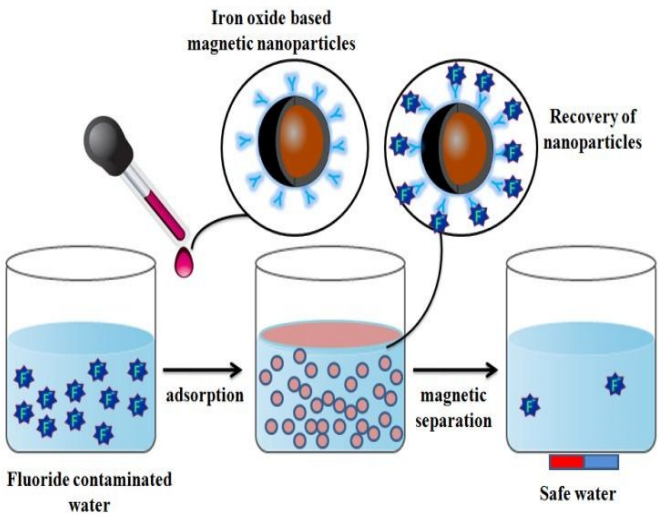

Fig. 3 Pictorial representation of the magnetic separation of nanoparticles after the completion of fluoride adsorption

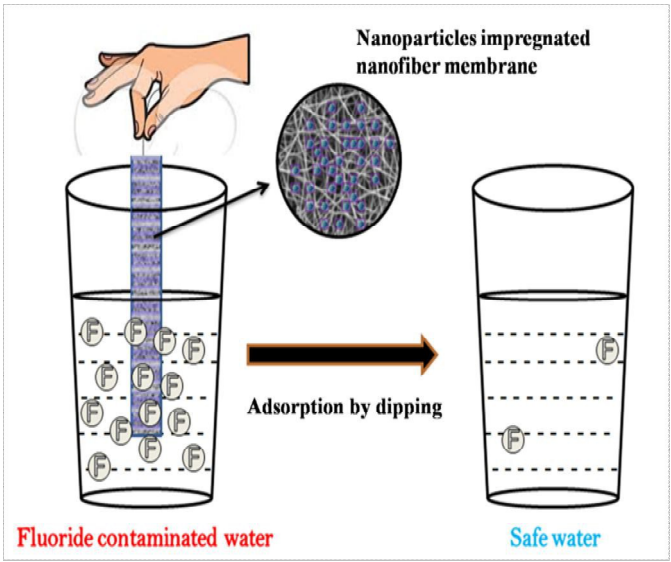

Fig. 4 Pictorial image of fluoride adsorption using nanoparticles impregnated nanofiber membranes by dip mode adsorption method. Adapted from ref 68 with permission from the Royal Society of Chemistry.

2.3. Polymer, carbon and hydroxyapatite based nanomaterials

The incorporation of nanomaterial into the polymer matrix increases the stability of the materials for fluoride adsorption. The fluoride adsorption by Al- and Fe-doped nano (~100 nm) sized porous polymeric adsorbent beads was reported by Kumar *et al.*[65] The material produced by suspension polymerization method possessed significant adsorption of F^- (100 mg/g). The fluoride adsorption studies performed by Mahapatra *et al.*[66] using electrospun alumina nanofibers showed maximum fluoride adsorption capacity of 1.2 mg/g. The nanoparticle impregnated hybrid nanofibers have unique and interesting features such as high surface area to volume ratio, large porosity, good mechanical properties, good water permeability and increased elution quality due to complete solid/liquid separation, which makes them suitable for drinking water treatment applications.[34,35,67] The nanoparticles impregnated nanofiber membranes can be used for fluoride removal through simple dip mode adsorption in future. Recently, hybrid Al_2O_3/Bio-TiO_2 Nanocomposite was prepared by our group and further impregnated onto thermoplastic polyurethane (TPU) nanofibrous membrane and studied for their efficiency towards fluoride removal from aqueous solution using dip mode adsorption method.[68] The adsorption capacity (Q_0) of the nanocomposite and the nanocomposite impregnated TPU nanofiber was found to be 2.73 and 1.9 mg/g respectively. This facile approach of designing nanocomposite impregnated nanofiber membrane can be used for F^- removal from drinking water. In **Fig. 4** the pictorial image will give an idea about the process of F^- removal using simple dip mode adsorption. This type of fluoride adsorption will be a quick process, safe, portable and of easy operation. Similarly the incorporation of zirconium (IV) tungstophosphate (ZrWP) ion exchanger into the chitosan biopolymeric matrix, synthesized by Viswanathan and Meenakshi[69] showed excellent defluoridation efficiency. Adsorption/complexation and ion exchange mechanism was reported as possible mechanism for fluoride adsorption by ZrWPCs composite (**Fig. 5a)**.The positive charges like Zr^{4+} and W^{6+} onto the nanocomposite surfaces attracts the negatively charged fluoride ions by means of electrostatic attraction as well as surface complexation. Further the $-PO_4^{3-}$group present in ZrWPCs composite act as a charge carrier which may get exchanged for F^- ions by ion exchange mechanism.

The novel nanoparticles impregnated carbon based adsorbents obtained by carbonization and activation of the natural materials possess appreciable defluoridation efficiency depending on the specific surface area, mesoporous structures and specific surface charge of the adsorbents[23-25]. The titanium and lanthanum oxides impregnated on granular activated carbon (TLAC) developed by Jing *et al.*[70] showed maximum fluoride adsorption capacity of 27.8 mg/g. The nanomaterial can be used as an effective adsorbent for simultaneous removal of F^-, As (V) etc. Materials like titanium and lanthanum oxides evenly distributed on the surfaced of the TLAC, preferably forms inner-sphere surface complexes with F^- ions and involve in F^- adsorption. Gupta *et al.*[71] developed a micro nano hierarchal web (MiNaHiWe) consisting of activated carbon fibers (ACF) and carbon nanofibers (CNF), impregnated with Al for the removal of fluoride from wastewater. Ma *et al.*[72] reported the fluoride adsorption property of manganese oxides impregnated granular activated carbon (GAC-MnO_2) using a redox process. The fluoride adsorption capacities of GAC-MnO_2 exhibited three times greater efficiency than uncoated GAC. pH of the solution influenced F^- removal. Zirconium impregnated activated charcoals prepared by Janardhana *et al.*[73] showed 3–5 times higher efficiency in the F^- adsorption when compared to plain activated charcoal. The mesoporosity and surface charge of the material influenced fluoride sorption very effectively. Similarly the amorphous Alumina-modified expanded graphite (Al_2O_3/EG) nano composite with a diameter of 10–30 nm was prepared using facile solution method followed by thermal treatment.[74] The maximum adsorption capacity was found to be 1.18 mg/g which is due to the generation of abundant hydroxyl ions on the surface of the adsorbent material (**Fig. 5b**). Aligned carbon nanotubes (ACNT) were used for the F^- adsorption studies by Li *et al.*[75] They found that the material has the adsorption capacity of 4.5 mg/L with 15 ppm of fluoride at pH 7. Higher positive surface charge of the material increases the tendency of the material to adsorb negatively charged fluoride ions. Both intra-particle diffusion and pore diffusion also play important roles in F^- adsorption process. If the radius of F^- is smaller than pore size of the adsorbent, increased the penetration of F^- into the inner layer of the synthetic adsorbents is possible which can make them a potential candidate for drinking water defluoridation process.[76-77]

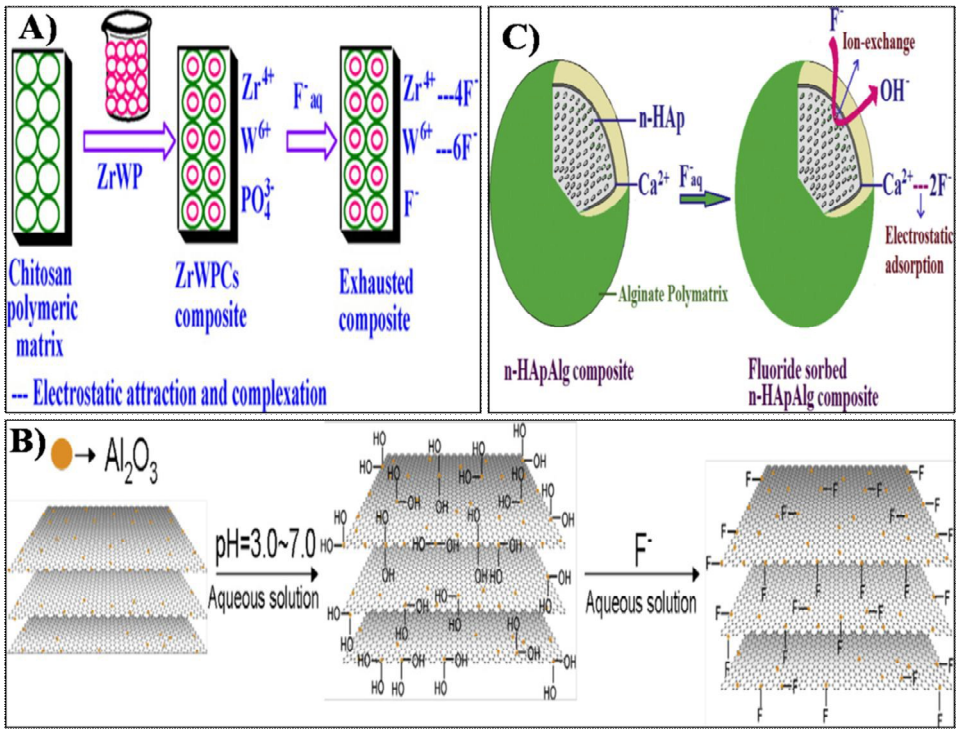

Fig. 5 Adsorption and ion exchange mechanism of fluoride adsorption by **(A)** ZrWPCs composite, **(B)** Alumina-modified expanded graphite (Al_2O_3/EG) nanocomposite **(C)** Alginate bioencapsulated nano-hydroxyapatite composite. Reprinted from ref 69,74 and 81 with permission from Elsevier.

Recently hydroxyapatite (HAp) based nanomaterial and its composites revealed very good prospective for defluoridation from aqueous solution. It was found that nano sized HAp were more efficient than the bulk due to its high surface area, porosity and high reactive surface charges. The simple wet chemical method of developing low cost nano-HAp was studied for fluoride adsorption by Sundaram *et al.*[78] and the results revealed that the maximum fluoride adsorption were about 1845 mg F^-/kg. The removal of fluoride ion by the nano-HAp was mainly due to both ion-exchange and adsorption process.

The fluoride adsorption using nano-HAp developed by combined ultrasonic and microwave technique was reported by Poinern *et al.*[79] which showed maximum monolayer adsorption capacity of 5.5 mg/g. Nano-HAp can be modified using various dopants to increase its fluoride adsorption efficiency than native HAp. Zhang *et al.*[80] studied hexagonal structured pure nano-HAp with particle size of about 20 nm × 60 nm for fluoride adsorption at various reaction temperatures. In this study, monolayer adsorption efficiency of HAp at different temperatures was found to be 19.742, 26.108, 36.914 and 40.818 mg/g for 298, 308, 318 and 328 K respectively. Alginate bioencapsulated nano-hydroxyapatite composite (n-HApAlg) was studied for fluoride adsorption by Pandi and Vishwanathan.[81] The nanocomposite showed excellent fluoride adsorption. The both adsorption as well as ion-exchange was the main mechanism of fluoride removal by n-HApAlg composite as shown in **Fig. 5 (c).** The mechanism reveals that the positively charged Ca^{2+} present in the nanocomposite gets attracted by negatively charged fluoride ions by means of electrostatic attraction. The OH− ions of the n-HAp lattice are replaced by the F^- ions by means of ion-exchange mechanism which further induced the fluoride adsorption property of the nanocomposite. As reported earlier, the electrostatic interaction and hydrogen bond are the main driving force for fluoride uptake onto HAp. The nanomaterials like nano-hydroxyapatite/chitosan (n-HApC) composite,[82] cellulose/HAp nanocomposites,[83] aluminum-modified HAp[84] and cationic surfactant modified HAp[85] are widely used for better fluoride adsorption than native nano-HAp. At low pH conditions, the HAp nanomaterials were protonated to positively charge that could attract fluoride anions by electrostatic attraction. Under neutral pH, the intra-particle diffusion and the ligand exchange process helps in the fluoride removal during adsorption. Thus the HAp based nanomaterials play a vital role in the fluoride adsorption studies.[23-25] Table 1 gives the summary of the F-adsorption capacity of various nanomaterial based adsorbents.

Table 1 Summary of the Maximum F^- removal capacities by different adsorbents

s. no	Nano-adsorbents	Nanomaterial characteristics	Working pH	AC mg/g	Short Summary	Ref
1	Nano-alumina	CP: α alumina; SA: 151.7m^2g^{-1}; PV: 1.09cm^{3g-1}	6.15	14.0	Adsorbent: commercial grade (Sigma–Aldrich). The batch sorption of F^- on nano-alumina was found to be strongly pH dependent with maximum F^- removal occurring at pH 6.15. The interaction between F^- and nano-alumina moieties result in the formation of aluminum-fluoro complexes. F^- sorption was influenced more by the presence of PO_4^{3-}, $SO_4^{2-}$and CO_3^{2-}.	43
2	Nano-AlOOH	CP: boehmite; CS: 133 Å; M: wire-like fibre(Dia: 15–25 nm); S A: 240.38 m^2g^{-1}	7	3.259	In batch mode, F^- removal efficiency was greater than 90% between pH 6 and 8 and decreased as pH values increase to 11. The presence of SO_4^{2-}or PO_4^{3-} in aqueous solution has been found to reduce the F^-uptake. Desorption studies showed that F^- can easily be desorbed at pH 13.	86
3	Nano-MgO	PS:18 nm; S A: 92.46 m^2g^{-1}; P V: 0.4313 cm^{3g-1}	10-11	14.0	Adsorbent: Commercial grade (Sigma–Aldrich). F^- adsorption studies were performed by batch mode. The F^- adsorption by nano-MgO was less sensitive to pH variations. At 0.6 g/L dosage concentration, maximum (90%) F^- removal was obtained. F^- sorption was mainly influenced by the presence of hydroxide followed by sulphate, bicarbonate and chloride.	41
4	Nano-sized goethite (ά-FeOOH)	PS: 1–10 nm; CP: α FeOOH	6-8	59	Adsorbent preparation: Precipitation method. The batch adsorption studies fitted well to pseudo-second-order kinetic model. The isothermic data showed good fit to Freundlich isotherm model. Contaminated ground water sample containing 10.25 mg L^{-1} fluoride could be purified in three stages using 8 g L^{-1} adsorbent dose.	87
5	CeO_2–ZrO_2 nanocages	PS: 80–100 nm; M: Hollow nanospheres/nanocages; CP: fcc; SA: 29.61 m^2g^{-1}	4.0	175	CeO_2–ZrO_2 nanocages were prepared by Kirkendall process, and their F^- removal performance was investigated in batch studies. The adsorption mechanism of the adsorbent for F^- involves anion exchange and electrostatic interaction.	88
6	Mn–Ce oxide nanocrystals	PS: 4.5 nm; S A: 41m^2g^{-1}	6	79.5	Adsorbent Preparation: Co-precipitation method. The adsorption was fast within the initial 1 h. The surface hydroxyl group density on the Mn–Ce adsorbent was mainly responsible for its high sorption capacity for F^-. Both anion exchange and electrostatic interaction were involved in the sorption of F^-	89
7	hydrous Ce(IV) + Zr(IV) mixed oxide nanoparticles (HCZMO)	CP: tetragonal; CS: 55–65 nm; PS: 60–70 nm; SA: 185.047 m^2g^{-1}; P V: 0.1219 cm^{3g-1}	5.8	12.4	HCZMO was prepared by low temperature and green method. Kinetic of F^- adsorption followed pseudo-second order kinetic model. Low activation energy (1.16 kJ mol^{-1}) and high adsorption energy (15.05 kJ mol−1) indicated high affinity of fluoride at HCZMO surface. >95% of desorption achieved using 1.0 M NaOH solution.	50
8	mesoporous $CoAl_2O_4$ nanoparticles	CP: hexagonal; SA: 379 m^2g^{-1}; P V: 0.984 cm^{3g-1} ; PD: 1.035 nm	7	14.80	Adsorbent Preparation: Micro-emulsion method. The high fluoride adsorption was mainly attributed to the adsorbent high specific surface areas and abundant pore structures.	90
9	Fe–Ti bimetallic oxide/Fe3O4 particles coreshell nanocomposite	M: core–shell nanostructure (dia:10–20 nm .shell thickness: 4.7 nm)	-	57.22	Adsorbent Preparation: Co-precipitation method. Batch adsorption studies indicated that the adsorption process was fast and reached equilibrium within 2 min. The nanoadsorbent was superparamagnetic with a saturation magnetization of 18.4 emu/g. This allowed rapid separation of adsorbent from water using external magnet.	91
10	CeO2/Al2O3 nanoporous composites	M: irregular sheet like structure ; SA: 266.1 m^2g^{-1}	3–10	37.0	Adsorbent Preparation: Co-precipitation method. During batch adsorption process, The coexisting anions had little effect on the F^- adsorption, except HPO_4^{2-} and $C_2O_4^{2-}$. The F^-adsorption followed pseudo second order kinetic model and Redlich-Peterson model isotherms	46
11	Bio Tio_2 nanoparticles	CP: anatase; M: spherical; PS: 47.26 ±13.5 nm	7	0.85	Adsorbent Preparation: microbial synthesis.	27
12	Fe-Al-Ce nano adsorbent	M: Agglomerated tiny granules of size 2–3 mm	7	2.22	Adsorption method: Column mode. 300 bed volumes can be treated with the effluent F^- below 1 mg/L for an influent F^- concentration of 5.5 mg/L, pH of 5.8, and SV of 5 h^{-1}. The coating of Fe–Al–Ce adsorbent can produce granules that can be used in a packed bed for the removal of F^- from drinking water.	92
13	Hydrous Iron(III) – Chromium(III) Mixed Oxide (HICMO)	M: agglomerated spherical nano particles (Dia: 40–55 nm)	6.5	16.34	Adsorbent Preparation: Co-precipitation method. The ion-exchange mechanism was suggested for the fluoride adsorption process. The adsorption reaction was endothermic and spontaneous. The high bicarbonate reduced the fluoride removal efficiency of HICMO.	48

	nanoparticles					
14	activated nano-gibbsite	CP: χ alumina; M: spherical; S A: 399 m^2g^{-1}	6	39	The increased surface area resulted in high fluoride sorption capacity (4×10^{-6} mol/m^2) which is equal to 39 mg/g. No pH or ionic strength dependency was observed in the pH range 4–6.5, suggesting an inner-sphere binding mechanism for low surface loads (0.526 mM).	93
15	nanosized fluorapatite (nFAP)	M: cylindrical rod like shape (Dia: 50–60nm)	3.0	7.45	Adsorbent Preparation: Solution-precipitation method. Adsorption of F^- by nFAP was fast and reached equilibrium in 120 min of contact time. Increase in the initial F^- concentration could effectively increase the F^- adsorption capacity.	94
16	Highly ordered mesoporous alumina	CP: α alumina; CS: 7~10nm, PS: 150~400nm S A: 163~338 m^2g^{-1} P S: 7~14nm	6.0	135	The adsorbent had high surface area and hydroxyl groups along with ordered mesoporous tunnel which favored diffusion and transportation of fluoride species.	95
17	magnesium oxide (MgO)-coated magnetite (Fe_3O_4) nanoparticles	M: core–shell nanostructure (Dia: 98.3 nm)	5-7	10.96	Adsorbent preparation: Sol-gel method. Maximum removal of F^- was estimated as 98.6% for an initial adsorbate concentration of 13.6 mg/L at optimal conditions: pH 6.0, adsorbent dosage of 2 g/L and contact time of 120 min by batch process	60
18	Fe3O4@Al(OH)3 magnetic nano-particles	CP: bayerite; PS: 240–340 nm; SA: 147 m^2g^{-1}	6.5	88.48	Adsorbent Preparation: Chemical co-precipitation method. Sorbents had higher surface areas and shorter diffusion route and the $Al(OH)_3$ surface layer of Fe_3O_4@$Al(OH)_3$ NPs possessed specific affinity toward fluoride.	61
19	CTAB mediated Mg-doped nano Fe_2O_3	CP:hematite; M: spherical; PS: 40 to 200 nm	7	75.2	Adsorbent Preparation: Surfactant mediation–precipitation method. The F^-adsorption studies were carried by varying time, pH, temperature and amount of adsorbent and adsorbate. The contaminated water collected from Nayagarh district of Orissa was defluoridated in a single stage batch mode.	51
20	Sulfate-doped Fe_3O_4/Al_2O_3 core shell nanoparticles	SA: 63.37 m^2g^{-1};M: nano-needle/spheres; PS:15-20 nm; SM: 16 emu/g	7	70.4	Adsorbent Preparation: Chemical co-precipitation method. Anion exchange of sulfate by F^- and formation of inner-sphere fluoride complex were the important mechanisms for fluoride removal by the sulfate-doped Fe_3O_4/Al_2O_3 nanoparticles	56
21	Fe–Ti bimetallic oxide nanoparticles	M: nano-needle/sphere granules; PS: 5–7 nm.	-	47.0	Adsorbent Preparation: Co-precipitation method. During batch adsorption, Fe and Ti in the Fe—Ti oxide adsorbent interacted synergistically to give increased F^- adsorption capacity higher than that of pure Fe oxide and Ti oxide adsorbent	96
22	Fe–Al-impregnated granular nanoporous ceramic	M: white and carmine colour spherical nanoporous particles (Dia:2-3 mm); S A: 40.22 m^2g^{-1}; P V: 0.078 cm^{3g-1} ; PD: 5 to 60 nm	4-9	3.56	More than 96 % removal of fluoride was achieved within 48 h from 10 mg/L initial fluoride solution at neutral pH by batch adsorption process. The F^- removal efficiency was significantly decreased in the presence of carbonate and phosphate anions.	97
23	Al- and Fe-doped micro/nanoadsorbent	M: smooth bead morphology; SA: ~750 m^2g^{-1}; PS: ~200 nm	7.4–8.0	~100	Adsorbent Preparation: Suspension polymerization method. The methodology adopted in this study to prepare bi-metal porous adsorbent toward developing multi-functional adsorbents	65
24	polypyrrole/Fe_3O_4 magnetic nanocomposite	M: agglomerated spherical nano particles (Dia: 10 nm); SA: 1206.53 m^2g^{-1}	6.5	22.3	The F^- uptake was very rapid and depended on the initial concentration, temperature, adsorbent dose and pH. Adsorption of F^- was not affected due to the presence of other anions such as chloride, nitrate, sulphate and phosphate.	62
25	Nanomagnetite aggregated schwertmannite	M: pincushion structure(width: 2–4 nm; length: 60–90 nm); SA: 276.15 m^2g^{-1}; PV: 0.139 cm^{3g-1}; PD: < 40 nm	5.8	17.24	Adsorbent Preparation: chemical precipitation/Wet chemical process. The permissible limit defined by WHO for defluoridation was achieved using 2 g/L adsorbent dose within 90 min contact time at pH 5.7 in batch adsorption process.	98
26	Zr–PAM/Fe_3O_4 nanocomposite	M: microporous (irregular pattern); SA: 124.5 m^2g^{-1} SM: 4.5 emu/g	3	124.5	The adsorbent developed had super paramagnetic properties of Fe_3O_4 nanoparticles and rapid F^- sorption property. Repeated sorption–regeneration cycles indicated reusability of the sorbent for F^- removal	64
27	Iron oxide-hydroxide nanoparticles	CP: orthorhombic; M: flower structure with several strings extended; PS: 20 nm; SA:6.57 m^2g^{-1}	-	1.66	The adsorbent showed good F^- removal. There is no significant influence of other co-anions like chloride, iodate, iodide and sulphate on the defluridation capacity of the nanoparticles except OH^-. The F^- adsorbed nanoparticles was regenerated upto 70% using Sodium hydroxide or hydrochloric acid solution.	44
28	lanthanum-impregnated activated alumina (LAA) nanoflakes	CP: amorphous; M: thin flakes (5-20 nm thickness; SA: 31. 235 m^2g^{-1}	3.9 to 9.6	16.9	LAA could adsorb 70.5–77.2% F^- in the pH range of the actual groundwater, about four times higher than activated alumina. Meanwhile, the Al release can be substantially reduced due to LaOOH formation. In addition, LAA can be regenerated and reused.	99
29	Mg–Al-LDH nanoflake	M: nanoflakes (thickness: 18 nm; dia:20 nm)	5.0	32.4	Mg–Al-LDH nanoflakes with a higher adsorption capacity for F^- were immobilized into alginate beads without leaching,	63

	impregnated magnetic alginate beads (LDH-n-MABs)				taking the safety issues of nanomaterials into consideration. Beads had a high magnetic sensitivity to an external magnetic field providing an easy and efficient way to separate them from aqueous solution	
30	Alumina Nanofibers	M: ultrafine cylindrical smooth nanofiber (dia: 200−600 nm)	7	1.2	Adsorbent preparation: Electrospinning method. Adsorption of F^- ions onto the alumina nanofiber surface followed Freundlich isotherm model indicating heterogeneous adsorption process.	66
31	Nanoporous Mg–Al–CO_3 layered double hydroxides	-	6.0	80.12	Adsorbent preparation: Co-precipitation method. The maximum removal of F^- from aqueous solutions was obtained in 6 h at pH 6.0 with an initial concentration of 50 mg/L, and that the retention of F^- ions by the material was 98%. The influence of co-existing anions in F^- aqueous solution indicated that the percentage of removal of F^- increases in the order $PO_4^{3-}<Cl^- \approx SO_4^{2-}<Br^-<<NO_3^-$ respectively.	100
32	aluminum-impregnated micro-nanohierarchal web (MiNaHiWe) of carbon fibers	M: smooth narrow range nanofiber (dia: 30−40 nm; length : several micrometers)	6	17.0	Adsorbent preparation: Chemical vapor deposition. The materials has been tested for the adsorption of F^- ions over the concentration range of 1-50 ppm in water under both batch and flow conditions. The adsorbent web showed significant adsorption of F^- ions. In addition, the total F^- uptake was observed to be higher on aluminum impregnated ACF/CNF web than on its parent material.	71
33	polyacrylonitrile coated with iron oxide nano particles	-	-	250	The influences of contact time, initial F^- concentration, and adsorbent dosage were investigated by batch equilibrium studies. The rate of adsorption was rapid with equilibrium being attained after 100 min.	101
34	Aluminium-Cerium alginate mixed metal oxide nanomaterial	PS: 3.14 nm; S A: 89.23 m^2g^{-1}; P V: 0.202 cm^{3g-1} ; PD: 46.32 Å	-	1.438	The material was able to remove 98% of F^- at natural pH of water bodies (pH = 7.0) Adsorption process followed pseudo-second-order kinetics and Freundlich isotherm.	102
35	ZnCr layered double hydroxides	CP: hydrotalcite; S A: 12-26 m^2g^{-1}; PV:0.04-0.11 cm^{3g-1}; PD: 135-173 Å	3-10	31	Adsorbent Preparation: Co-precipitation method. Adsorption studies: Batch and column mode. The uptake capacity of the composite materials increased with an increase in LDH content in both batch and column studies. Further, the composite materials showed better aqueous diffusivity than powdered materials.	103
36	Fe(III)–Zr(IV)Zr)–alginate (FZCA) micro/nanoparticles	-	7	0.981	The sorption of F^- followed pseudo-second order kinetics. The positive value of thermodynamic parameter (ΔH^0) indicated increasing randomness during the sorption process. The desorption characteristic of the hybrid material shows that nearly 89% of F^- could be leached out at pH 12.	104
37	nano-size hydroxyapatite	M: needle-shaped crystals (dimensions of 50−100 nm)	5.0	0.489	Suspensions of HAp (2 gL^{-1}) were equilibrated under controlled pH conditions (pH 6.5, 7.3, 9.5) at 25 °C for 28 d after the addition of different F^-concentrations (0.5−7.0 mM). Analysis of the reacted adsorbent indicate that a fluoridated surface layer with a thickness of several nanometers was formed on nanosized Hap.	105
38	Cellulose@hydroxyapatite (HA) nanocomposites	M: irregular flakes; CS: 20–50 nm; SA: 76.257 m^2g^{-1}	6.5	4.2	Adsorbent Preparation: Insitu hybridization method. Adsorption equilibrium of F^- was reached within 360 min. The coexisting anions like nitrate, sulfate and phosphate had no significant effect on F^- adsorption.	106
39	Chitin–nano-hydroxyapatite composite (n-HApCh)	-	7	8.4	Adsorbent Preparation: Co-precipitation method. The main advantages of n-HApCh composite are biocompatible, low cost material, indigenously synthesized and can be effectively utilized as promising defluoridating agent.	82
40	Li−Al layered double hydroxides	CP: hexagonal/ monoclinic, M: rosette-shaped particles	6-7	47.24	The maximum percentage removal (97.36%) could be reached and the adsorption equilibrium could be attained within 1 h. Based on FT-IR and kinetic analysis, the "memory effect" may play an important role in the early adsorption stage, while the ion-exchange process may control the adsorption rate at the second stage adsorption.	107
41	Mg/Fe layered double hydroxides	M: wizened nanosheets (Dia: 100 nm)	7	28.65	Adsorbent Preparation: Hydrothermal process. When compared with commercial activated alumina, the synthesized adsorbent was devoid of potential risks associated with alumina and had a lower leaching of metal ions. Maximum F^- desorption of 97.2% was achieved	108
42	Hybrid Al_2O_3/Bio-TiO_2Nanocompo	CP: orthorhombic (alumina), Anatase/rutile (titania); PS: 50±6 nm.	7	2.73	Adsorbent Preparation: Microbial and chemical method Adsorption method : batch process. The adsorption capacity was reported to be 2.73 mg/L.	68

	site					
43	Hybrid Al_2O_3/Bio-TiO_2Nanocomposite impregnated TPU nanofiber membrane	M: smooth narrow range nanofiber (dia: 239+33 nm, thickness: 21.94 ±1.3μm,); swelling ratio: 6.02 ± 0.7 %; porosity:43.34± 4.3 %)	7	1.9	Adsorbent preparation: Electrospinning/spraying, Adsorption method: Dip mode process. The adsorption capacity was reported to be 1.9 mg/L.	68
44	MWCNTs	-	5	3.50	The performance of the MWCNTs was good at lower F^- concentrations (less than 2 mg/L).	109
45	ZrO_2 hybrid CNTs	-	-	60.57	Adsorbent preparation: Microwave assisted process. Fluoride uptake reached 79% of the equilibrium value within the first five minutes, indicating high rate of adsorption. The fluoridated ZrO_2/MWCNT could be regenerated easily by treating with an alkaline solution.	110
46	CNTs supported Alumina	SA: 165 m^2g^{-1}: PV:0.176 cm^{3g-1}; PD:4.26 nm	6.0–9.0	24.15	Adsorption capacity was maximum at alumina loading of 30 wt%. All adsorption isotherms at different pH followed Freundlich model. Kinetic studies shows that fluoride adsorption onto Al_2O_3/CNTs was a second order rate reaction.	111
47	CTAB functionalized MWCNTs	SA: 75.2m^2g^{-1}: PV: 0.0925 cm^{3g-1}; PD:5.2 nm	2-11	20.10	A novel CTAB grafted MWCNT (CGCNT) adsorbent was synthesized by a green route using ultrasonication and using a green solvent (isoamyl alcohol). It was found that the removal of F^- could be achieved over a wide range of pH from 2 to 11. This could be attributed to the positive zeta potential of the CGCNTs in both acidic and basic medium. The recyclability and applicability of the adsorbent to F^- spiked high alkaline ground water was also demonstrated.	112
48	Amorphous Alumina-modified Expanded Graphite (Al_2O_3/EG) nanocomposite	M: peas-like structure (Dia: 10-30 nm, length:20-50 nm)	3-7	1.18	Adsorbent preparation: solution method followed by thermal treatment. With the optimum parameters of the batch adsorption experiment (Initial F = 5 mg/L, pH = 4.0, Temperature = 30 ºC, time = 120 min and adsorbent dosage = 0.2 g) the removal rate was 94.4%. The adsorption was multi-molecular layer.	74
49	Aligned carbon nanotubes(ACNTs)	Diameter-20-80 nm; SA: 72 m^2g^{-1}: PV: 0.15 cm^{3g-1}; PD:3.8 nm	7.0	4.5	Adsorbent preparation: Catalytic decomposition method. The kinetics experiment of ACNTs shows that fluoride adsorption rate is fast in the first 60 min and reaches equilibrium gradually in about 180 min. The highest adsorption capacity of ACNTs was 4.5 mg/g at pH 7 with fluoride concentration of 15 mg/L.	75
50	aluminumsulfate and graphene hydrogel (BAS@GHG) nanocomposite	CP: amorphous; M: spherically shaped GHG onto CCG 2D thin sheets.	7.2	33.4	Adsorbent preparation: Homogeneous precipitation method. In the adsorbent, the presence of BAS was believed to provide high F^- adsorption capacity through ligand exchange mechanism between hydroxide ions and F^- ions. Simultaneously the GHG acts as a porous matrix which can provide large surface area and facilitate the diffusion of adsorbate.	113

CP: crystalline phase; SA: surface area; PV: pore volume; M: morphology; PS: particle size; PD: Pore diameter; SM:Saturation magnetization

3. Advanced nanomaterials for nitrate removal

Similar to the technological applications of nano based adsorbent materials available for fluoride removal; extensive research has attracted many researchers in recent years for nitrate removal from aqueous solution. When compared to other methods like biological nitrate reduction[7], adsorption and photocatalytic process are widely used to remove NO_3^- very effectively from water. Various advanced nanomaterials used for the adsorption and photocatalytic degradation of nitrates and their reacting mechanisms are discussed in the following sections.

3.1. Nanomaterials for nitrate removal by adsorption

Selection of a suitable adsorbent media for NO_3^- removal from aqueous solution is similar to that of fluoride due to their identical ionic charge. The mechanism of nitrate adsorption by various nanomaterials is based on the electrostatic attraction or ligand-exchange reaction between nitrate and hydroxyl ions depending on the pH of the medium.[114,115] Recently, the feasibility of nano-alumina for NO_3^- removal from aqueous solutions was explored by Bhatnagar *et al.*[116] The maximum sorption capacity of nano-alumina for NO_3^- removal was found to be 4.0 mg/g. The ligand exchange reactions between the nitrate ions and surface charge of the adsorbent material took a major role in the NO_3^-adsorption process. Zhang *et al.*[117] synthesized a highly porous nanocomposite material consisting of MgO nano-flakes within the biochar matrix for the removal of nitrate from water. The nitrate adsorption capacity for this material was found to be 95 mg/g. The nano-flake structures were regular in morphologies and dispersed uniformly on the surface of the biochar matrix and made it a potential candidate for nitrate removal from aqueous solution.

Saad *et al.*[118] synthesized amino-functionalized mesoporous silica materials and successfully applied them to remove NO_3^- from water. The aminated and protonated mesoporous silica

showed high adsorption capacity for nitrate reaching 46.5 mg/g compared to adsorption capacity of 2.4 mg/g for the unmodified mesoporous silica. Fe_3O_4/ZrO_2/chitosan nanocomposite having the surface area 212.9 m^2/g was prepared by Jiang *et al.*[119] using simple wet chemical method and studied for its NO_3^- adsorption ability. The material exhibited maximum NO_3^- adsorption of about 89.3 mg/g and was attributed to the physical forces besides electrostatic interaction during adsorption. It also been noted that the saturated Fe_3O_4/ZrO_2/chitosan nanocomposite adsorbent cannot be thoroughly regenerated by strong alkali condition. Graphene oxide (GO) coated Fe, Ni and Co nanoparticles were prepared by Motamedi *et al.*[120] using simple chemical reduction method which showed good NO_3^- removal efficiency. According to the author the NO_3^- adsorption efficiency of Fe-GO was higher than that of the reported unanchored Fe nanoparticles. Similarly, the Ni-GO and Co-GO showed notable nitrate removal potential similar to that of Fe-GO. This observable fact is attributed to the greater dispersion of pure zero-valent Ni and Co over GO. It is also proved that this material is highly efficient in the adsorbing NO_3^- due to its magnetic property and oxidation potential nature. The quasi-spherical shaped Fe NPs were successfully synthesized by Wang *et al.*[121] via facile one-step, biosynthetic route using green tea (GT) and eucalyptus leaf (GL) extracts. The maximum nitrate adsorption efficiency was found to be 13.06 mg/g for GT-Fe and 9.698 mg/g for EL-Fe NPs. The efficiency was further compared with the native zero-valent iron nanoparticles (nZVI) and Fe_3O_4 nanoparticles which had 87.6% and 11.7% nitrate removal respectively. The adsorption of nitrate by Pd/Cu supported on active carbon bimetallic materials was studied by Mikami *et al.*[122] The results revealed that the NO_3^- was strongly adsorbed on specific Pd-Cu bimetallic sites.

Suitable metal oxides can be introduced into the CNTs to make efficient adsorbent materials for nitrate removal. The maximum adsorption efficiency of the nitric acid and liquid ammonia functionalized carbon nanotube (CNT) sheets were found to be 90.9 and 142.85 mg/g respectively. The results demonstrated that the nitrate adsorption by the modified CNTs sheets is only due to the strong electrostatic interactions between negative charge of NO_3^- and positive charge of the CNTs surface.[123] Similarly the NO_3^- adsorption capacity of powdered activated carbon (PAC) was compared with CNTs. The NO_3^-adsorption capacity of CNTs (25 mmol/g) was found to be higher than PAC (10 mmol/g).[124]

In recent research, efforts have been taken to impregnate nanoparticles or composite materials on suitable matrix in-order to increase the efficiency of adsorbent-adsorbate separation after the reaction without any gradual decrease in the adsorption capacity. Alumina nanoparticles with average diameter of 62 nm was impregnated on to the polyacrylonitrile mixed hollow fiber membrane which showed better nitrate adsorption capacity of 15 mg/g.[125] The pore size of the membrane and the charge of the alumina nanoparticles dually contribute to the nitrate removal efficiency in aqueous solution. The removal of nitrate on $ZnCl_2$ modified lignite granular activated carbon (LGAC) was investigated by Khan *et al.*[126] The maximum adsorption capacity was found to be 4.4 mg/g. The NO_3^- adsorption was mainly due to the active sites –C=OZn^{2+} and –COO–Zn^{2+}, rather than the –OH sites present on the material surface. Hence according to the author the NO_3^- adsorption by LGAC was due to the physical adsorption process. Hydrotalcite-like mesoporous compounds, also known as layered double hydroxides (LDH), constitute an important class of inorganic materials with desirable properties to remove NO_3^- from aqueous solution. The impregnation of various metals onto the LDH has increased the NO_3^- adsorption capacity. The Zn-Al-Cl and Mg-Al composite impregnated LDH has been synthesized by co-precipitation method and tested towards NO_3^- removal from water. The adsorption capacity was found to be 40.26 and 35 mg/g respectively. The percentage NO_3^- removal was found to decrease gradually with increase in pH and the optimum pH was found to be 6. The presence of competitive anions reduced the NO_3^- adsorption in the order of carbonate > phosphate > chloride > sulphate respectively. Thus the nature and content of divalent cations in LDHs provided a strong influence on the NO_3^- adsorption process. Similarly various metal impregnated mesoporous LDHs like Ni–Fe-LDH, Mg–Fe-LDH has been reported for the adsorption of nitrate from aqueous solution.[127,128] The biosorbents like chitin and chitosan-derivatives based mesoporous materials gained wide attention towards nitrate adsorption. High contents of amino and hydroxyl functional groups in these biosorbents were responsible for the significant adsorption potential towards nitrate. The adsorptive mechanism is mainly due to the electrostatic interactions between the negatively charged NO_3^- group and the positively charged amine group. The NO_3^- adsorption capacity of mesoporous chitosan hydro beads prepared by Chatterjee and Woo was found to be 92.1 mg/g.[129] Similarly microalgae immobilized on chitosan nanofiber mats were recently developed by Eroglu *et al.*[130] for the efficient removal of nitrate with its potential, simple and highly durable polymer capability. This type of bio-based nanomaterial which is water-insoluble and non-toxic support is needed for the efficient adsorption of nitrate from aqueous solution. The pH of the medium plays a major role in nitrate adsorption by most of the nanoadsorbents. At high basic pH, most of the materials do not favour the adsorption due to its electro static repulsion between the negatively charged adsorbent surface and the anion NO_3^-. At high acidic pH, the electrostatic attraction takes place between the positive charge adsorbent and the negative charge adsorbate and makes effective adsorption process. In neutral pH the nitrate adsorption is still possible by ion exchange and intraparticle diffusion process. Hence the nitrate adsorption process by nanoadsorbents mostly takes place by these three 1.ion exchange, 2.intraparticle diffusion and 3.electrostatic attraction between the adsorbent surface and the pollutant ion.

3.2. Nanomaterials for nitrate removal by photo catalysis

Photocatalytic removal of nitrates from drinking water using various nanomaterials is an important and developing area of

research. A number of research studies have reported that the photocatalytic reduction of nitrate in the aqueous solution could be achieved with high efficiency using various types of photocatalysts like TiO_2,[131] ZnO,[132] SiO_2[133] CeO_2,[134] SnO_2,[135] ZrO_2,[136] ZnS,[137] CdS[138] and nZVI.[139] The recent advanced nanomaterials used for the photocatalytic removal or reduction of nitrates are discussed below. Among the above, the TiO_2 nanoparticles have emerged as promising photocatalysts for water purification units especially in the removal of ions like nitrate, nitrite, arsenic, chromium etc.[140-141] TiO_2 nanoparticles are very versatile in nature and can act as both oxidative and reductive catalyst to degrade various pollutant ions present in the water. The photocatalytic removal of NO_3^- using titania based nanoparticles are well reported. In brief, illumination of TiO_2 surface with UV irradiation (<385nm) with energy greater than the band gap energy of the semiconductor TiO_2 (3.2 eV) generates valence band holes and conduction band electrons **(Fig. 6 (a)).**[144]Holes and electrons react with species adsorbed on the catalyst surface. Valence band holes reacts with water (H_2O/OH^-) to generate hydroxyl radicals (HO●), while electrons react with adsorbed molecular oxygen (O_2) reducing it to superoxide radical anion, which in turn, reacts with protons to form peroxide radicals. Hydroxyl radicals can further oxidize pollutants ions.[142-144] The above mechanism is proposed for the conversion of nitrate to nitrite and further to nitrogen/ammonia in the drinking water. The NO_3^- ions formed during the photocatalytic reaction further get reduced to form ammonia, which in turn, reacts with the valence band holes and decomposes to nitrogen gas. As we know generally, the titania exhibits in different crystalline phases like anatase, rutile and bookite. The photo catalytic efficiency of the titania may vary based on the crystalline phase, fermi level position, electron mobility, concentration of hydroxyl groups, electronic and surface properties. The bookite phase of titania is rare and also it is unstable in nature. The anatase is highly photo catalytic than rutile due to its structural differences, electronic band structures, subsequent charge transfer, different mass densities, recombination rate and average effective mass of photo-generated electrons and holes.[145-148] Therefore, it is not surprising that anatase usually shows a higher photocatalytic activity than rutile phase. The recent reports put in the picture that the mixed phase of anatase and rutile phases in the nanocrystalline TiO_2 nanoparticle shows superior photo catalytic efficiency when compare to the free anatase and rutile structured materials.[149-151] One of the best example is commercially available Degussa P25-TiO_2 nanoparticles having mixed anatase and rutile phases. This is generally attributed to the formation of n–p junctions at the phase interfaces which improves the efficiency of charge carrier separation.[152] Another requirement of the photocatalytic nitrate reduction processes is the addition of simple organic compounds which would act as an electron hole scavenger that provides electrons to fill the electron holes in the valence band. Previous studies reported that formic acid as one of the most efficient electron hole scavengers for nitrate reduction over TiO_2.[153-154]

One of the major challenges for the scientific and industrial community involved in photocatalytic research is to increase the spectral sensitivity of TiO_2-based photo catalysts to visible light. The TiO_2 nanoparticles are only sensitive to the UV radiations, because of which the photocatalytic reactions can take place only under UV light. This TiO_2 is further modified with various conductive metal nanoparticles to increase the efficiency of NO_3^- degradation under visible region. Jin *et al.*[155] studied that the metal Cu loaded catalysts, Cu/TiO_2 and Cu/$MgTiO_3$-TiO_2, exhibited higher photocatalytic activity, which indicated that metal loading onto the catalyst was essential for the reduction of NO_3^-. The composite semiconductor catalyst induces superior photocatalytic activity in the process of NO_3^- ion reduction. The composite formation and crystalline phase transformation of TiO_2 were the important factors in the NO_3^- reduction.

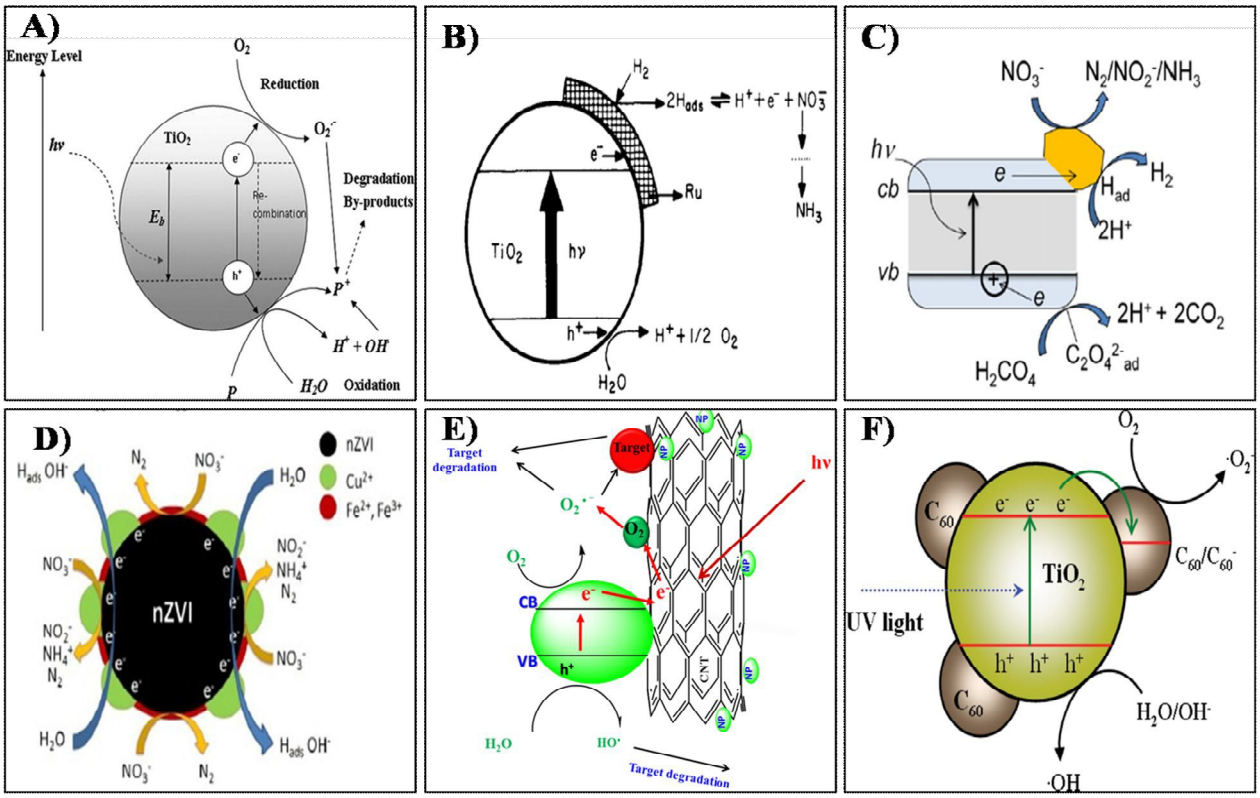

Fig. 6 Mechanism of photo catalysis by A) TIO_2, B) Ru/TiO_2, C) Au/TIO_2, D) Cu-nZVI E)metal oxide doped CNT and F) C_{60}/TiO_2 nanocomposite. Reprinted from ref 144,156, 163, 175, 192 and 193 with permission from Elsevier, Applied Environmental Research,INTECH, The Royal Society of Chemistry.

The ruthenium doped TiO_2 catalyst developed by Ranjit *et al.* [156] showed efficient nitrate degradation. The metal loaded on to the semiconductor catalyst can be advantageously used for hydrogenation/reduction reactions. The author exemplifies the NO_3^- degradation mechanism by photocatalytic reaction of nitrate into nitrite and further into ammonia by the Ru/TiO_2 catalyst. The scheme suggested for the reduction process by the catalyst materials is shown in the **Fig. 6(b).**[156] According to the author the photocatalytic reduction of nitrite and nitrate ions is dependent on many factors such as the nature of the metal loaded on the TiO_2, the nature of the sacrificial agent, pH of the medium and irradiation time. However, here the author could not observe any other intermediates in his photocatalytic experiments. The photocatalytic reduction of nitrate ions were investigated using pure TiO_2 and $Ag–TiO_2$ thin films prepared using simple sol-gel dip coating technique.[157] The optical band gaps of the TiO_2 and $Ag–TiO_2$ thin films were found to be 3.27 and 2.70 eV respectively. The net efficiencies of photocatalytic nitrate reduction of TiO_2 and 0.1% $Ag–TiO_2$ were 41.4% and 70.0%, respectively. Sa´ *et al.*[158] studied the simultaneous degradation of NO_3^- and organic acids using Ag/TiO_2. 100 % nitrate removal was achieved and the residual nitrite and ammonium levels were below the EU guideline levels. Similarly, report by Zhang *et al.*[159] states that using Ag/TiO_2 catalyst shows total nitrate conversion of 98% at a N_2 selectivity of 100%. This ideal metal doped TiO_2 gives better photocatalytic efficiency in the removal of NO_3^- when compare to plain TiO_2.

Likewise Au/TiO_2 composite material is extensively reported for the removal of NO_3^- using photo catalysis.[160-163] The incorporation of Au, results in the significant improvement in the photonic efficiency for titania catalyst due to the generation of Schottky barriers which inhibit the recombination of electron–hole pairs and the process under UV activation, which is represented by the schematic shown in **Fig. 6 (c).**[163] For the metals like Au, Cu, Ag a Schottky barrier is formed, thus electrons flow into the metal and become trapped. This allows electron storage, facilitating the multi-electron nitrate reduction reactions. Similar photocatlytic reduction of nitrates was reported by Rengaraj and Li,[164] Lozovskii *et al.*[165] and Doudrick *et al.*[166] However, the practicability of applying doped nano crystalline TiO_2 catalysts in photocatalytic water treatment needs reconsideration because of the low catalytic activity of the doped TiO_2 catalysts under visible light and the possibility of dopant leaching.

The use of nZVI based materials is one of the promising approaches in NO_3^- removal studies. Various studies have been done in the removal of NO_3^- using nZVI.[167-169] The reaction and its mechanisms between NO_3^- and nZVI is a true redox reaction.[170] Several studies have indicated that the final products of chemical reduction of NO_3^- by nZVI, could be N_2 or NH_3 depending on the experimental conditions. The

nanoscale zero valent iron supported on pillared clay (nZVI/PILC) was prepared and used for NO_3^- removal by Zhang *et al.*[171] The prepared nZVI of 30–70 nm particle size was evenly distributed along the clay phase. It was reported that using nZVI/PILC, almost all NO_3^- was converted to other nitrogen species, so the removal of nitrate by nZVI/PILC was dominantly attributed to the reduction by nZVI instead of adsorption by PILC. Similar conversion of nitrate into nitrogen gas has also been observed in various reports.[172-174] Enhanced nitrate reduction by copper impregnated nanoscale zero valent iron (Cu-nZVI) was reported by Krasae *et al.*[175] The results found that nitrate removal over Cu-nZVI was greater than that of nZVI. By coating nZVI with novel metal catalysts such as Pt, Pd, and Cu, the performance of nZVI toward nitrate removal was found to be increased. The possible reaction mechanism involved in bimetallic Cu-nZVI, for nitrate removal is illustrated in **Fig. 6 (d).** Hence coating of Cu can enhance nitrate removal performance since Cu is reduced by nZVI to Cu0 on the nZVI surface. Cu can effectively adsorb hydrogen produced from the reaction between nZVI and water, which can then react with nitrate to produce nitrite and continuously react to form ammonia and nitrogen gas. Liou *et al.*[176] found that Cu-nZVI shows higher photocatalytic efficiency than Pt and Pd loading because Cu can extract oxygen from NO_3^- and highly adsorb hydrogen with both adsorbed species reacting continuously. The photo catalytic removal of NO_3^- was performed by Pan *et al.*[177] using TiO_2, nano zero valent iron (nZVI) and nano-TiO_2–Fe^0 (NTFC) composites. The experimental results confirm that NTFC can effectively remove nitrate when compared to others. The composition of NTFC at 1:10 of TiO_2 to nZVI ratio greatly influences the conversion of nitrate to N_2, which can be attributed to the maintenance of high level of ferrous ions in the NTFC system due to its reducing condition. The efficiency of functional kaolinite, in supporting the Fe/Ni nanoparticles for the removal of NO_3^- was reported by Shi *et al.*[178] and Cai *et al.*[179] In this system, Fe^0 is said to act as the reducing agent, Ni and Cu act as the catalysts for the hydrogen generation and kaolin serves as a support. The results revealed that, by introducing nickel, the rate of nitrate degradation increases enormously. Removal of nitrate using nano SiO_2–FeOOH–Fe core–shell was studied by Ensie and Samad.[180] The loading of nZVIs was found to play a significant role in NO_3^- removal, by doubling nZVI loading, removal of NO_3^- increases from 69% to 86%. This type of core shell nanostructures increases their stability and also prevents agglomeration in reaction medium. Su *et al.*[181] studied doping of nZVI with Au, which resulted in significant reduction in nitrite yield ratio and was found to be much better than nZVI only, or doping nZVI with Cu or Ag. Catalytic hydrogenation of NO_3^- using bimetallic catalysts has been noted as a promising denitrification method. In these aspects the ZrO_2 supported Pd−Cu bimetallic catalysts were used for the photo catalytic removal of NO_3^-. The material containing high Pd/Cu ratio exhibits a high catalytic activity.[182] The palladium doped gold nanoparticles was prepared by Qian *et al.*[183] to study the catalysis mechanisms for NO_3^- reduction. The results revealed that bimetallic Pd-on-Au NPs had catalytic properties toward rapid and selective reduction of NO_3^-.

Various bimetallic catalyst nanomaterials like Pd-Cu/Al_2O_3,[184] Pd-Sn/Al_2O_3,[185] Pd-In/Al_2O_3,[186] Pd-Cu/TiO_2[187] and Rh–Cu/Al_2O_3[188] are reported for the efficient removal of nitrate with high selectivity and specificity. The catalytic behaviors of bimetallic catalysts can also be adjusted by using different supports. The membranes, fibers, resins and ceramics were used as the supports in bimetallic catalysts to circumvent the diffusion problem. Deganello *et al.*[189] selected pumice as the support to change the electronic properties of Pd sites to enhance nitrate reduction. Dual process like photocatalytic and adsorption can be achieved by hydrotalcite supported Pd-Cu catalyst due to the decreased mass transfer limitation by adsorption of nitrate in the interlayer of hydrotalcite and reduction by Pd-Cu catalyst. Roveda et al.[190] used acrylic resins as supports in Pd-Sn bimetallic catalysts to provide the buffering environment. The Pd-Cu bimetallic catalyst with ZrO_2 as the support was found to be more active as compared to SnO_2 supported Pd-Cu catalyst. $NaTaO_3$ nanoparticles were prepared by an ultrasonic method, and Pd was deposited onto the surface of $NaTaO_3$ via photo assisted deposition.[191] The different ratio of palladium composition in the nanoparticles yielded different properties. The crystallite size of $NaTaO_3$, 0.2 Pd/$NaTaO_3$, 0.4 Pd/$NaTaO_3$, 0.6 Pd/ $NaTaO_3$, and 0.8 Pd $NaTaO_3$ was found to be 15, 12, 10, 8 and 6 nm, respectively. Among the above ratios the 0.6 Pd/$NaTaO_3$ showed better nitrate degradation efficiency when compare to others. The author experimentally proved that the 1.2 g of 0.6Pd/$NaTaO_3$ in 1000 mL of a 100 mg/L nitrate solution yielded a nitrate reduction efficiency of 100% within 50 min of irradiation of visible light. An attempt was made by our group using co-electro spraying method to deposit TiO_2 nanoparticles on to the PAN nanofiber membrane for the photocatalytic removal of nitrates from aqueous solution.[15] The maximum nitrate removal was found to be 39% for the initial nitrate concentration of 10 mg/L. However at higher concentration, the TiO_2/PAN nanofiber membrane was inefficient to remove nitrate. Hence there is a need for alteration technique to coat nanoparticles on to the membrane that will not block the photocatalytic process.

The TiO_2 based semiconducting nanoparticles was impregnated onto the carbon nanotubes to increase the efficiency of the nitrate removal. CNTs can be used as a catalytic supporter in order to increase not only the specific surface area providing more hydroxyl radicals, but also the quantum efficiency by retarding charge carrier recombination and scavenging photo-generated electrons through the interface between TiO_2-carbon nanotube and make TiO_2 more sensitive to the visible light. The pictorial representation of the general photocatalytic activity of the metal oxide doped CNT is shown in the **Fig. 6(e).**[192] By considering this concept the efficient nitrate degradation may also be possible even in visible light. Yu *et al.*[193] reported that fullerene modified TiO_2(C_{60}/TiO_2) nanocomposite may also has better catalytic efficiency. C_{60} molecules can be dispersed as a monolayer onto bimodal mesoporous TiO_2 via covalent bonding. The C_{60} molecules

doped onto TiO_2 act as "electron acceptors" responsible for the efficient separation of photo-generated charge carriers and the enhancement of photocatalytic activity.[194-195] A schematic illustration of the mechanism of enhanced photo activity of the C_{60}/TiO_2 nanocomposite is shown in **Fig. 6(f).**[195] These separated electrons and holes are then trapped by surface catalysts and increase the recombination time in a favourable way. Hence the development of hybrid catalyst materials by using these types of functional materials can be well used for the photo degradation of nitrate molecules.

4. Conclusion

Various advanced nanomaterials used for the removal of fluoride and nitrate from aqueous solution have been summarized briefly in this review. This review gives the clear idea about the tuning of metal oxide based nanoparticles with suitable metal ions which might be helpful in the dual efficiency of adsorption and photocatalytic degradation for the removal of fluoride and nitrate. The alumina, iron oxide, LDH and HAp based hybrid nanomaterials have shown high fluoride and nitrate adsorption efficiency when compared to other nanomaterials. The metal dopents like Cu, Mg Ru Ag Au Pt, Pd influence the photocatalytic performance of the semiconducting nanomaterials like TiO_2, SiO_2 and CdS etc. Various conventional and non-conventional advanced nanomaterials have been assessed for the removal of fluoride and nitrate from water. Still many of them meets its own merits and demerits in practical application. The researchers have to choose a material which offer satisfactory results in removal of fluoride or nitrate to below permissible limit along with low cost, simplicity of design and operation.

Acknowledgement

The authors are thankful to PSG Management and PSG Institute of Advanced studies for their valuable support.

Notes and references

[a]Nanobiotechnology laboratory, PSG Institute of Advanced Studies, P.B. No: 1609, Peelamedu, Coimbatore 641004, India. Tel.: +91 422 4344000 extn 4321; E-mail: selvabiotech@gmail.com, *rsk@psgias.ac.in*

1. Zaporozec, *Geo Journal*, 1981,**5**,457-471.
2. R. E. S. Bain, J. A. Wright, E. Christenson and J. K. Bartram, *Sci. Total Environ.*, 2014,**490**, 509-513.
3. H. H. Dieter, Drinking-Water Criteria (Safety, Quality, and Perception) *Encyclopedia of Toxicology* (Third Edition), 2014, 227-235.
4. D. A. Birkholz, S. M. Stilson, H.S. Elliott. Reference Module in Earth Syst. Environ. Sci., **2**, 2014, 212-229.
5. E. Kumar, A. Bhatnagar, W. Hogland, M. Marques and M. Sillanpaa, *Adv. Colloid Interface Sci.*, 2014, **203**, 11-21.
6. A. Banerjee, *Geoscience Frontiers*, 2015,**6**, 277-284.
7. S. Kavitha, R.Selvakumar, M.Sathishkumar, K.Swaminathan, P.Lakshmanaperumalsamy, A.Singh and S.Jain *Water Sci Technol.*, 2009, **60(2)**, 517-524.
8. P. Denbesten and W. Li,*Monogr Oral Sci.*, 2011, **22**, 81-96.
9. M. Abdollahi and F. Momen-Heravi,Fluoride. Encyclopedia of Toxicology (Third Edition), 2014, 606-610.
10. Y. Zhou, H. Zhang, J. He, X. Chen, Y. Ding, Y. Wang and X. Liu,*Food ChemToxicol.*, 2013, **56**, 297-303.
11. O. Barbier, L. A. Mendoza, L. María and D. Razo,*Chem. Biol. Interact.*, 2010, **188**, 319-333.
12. K. Yang and X. Liang, *Encyclopedia of Environmental Health*, 2011, 769-775.
13. H. Liu, Y. Gao, L. Sun, M. Li, B. Li and D. Sun,*Int J HygEnvir Heal.*,2014, **217**, 413-420.
14. A. M. Fan, 2014.Nitrate. *Encyclopedia of Toxicology* (Third Edition), 523-527.
15. S. P. Suriyaraj, M. BenasirBegam, S. G. Deepika, P. Biji and R. Selvakumar. *Water Sci. Technol.: Water Supply*, 2014, **14**, 554.
16. S. Nathan, S. Bryan, D. Dominik, Alexander, J. R. Coughlin, A. L. Milkowski and P. Boffetta, *Food Chem. Toxicol.*,2012, **50**, 3646-3665.
17. N. E. Herrera, K. P. Cantor, N. Malats, D. T. Silverman, A. Tardón, R. García-Closas, C. Serra, M. Kogevinas and C. M. Villanueva. *Environ. Res.*,2015,**137**, 299-307.
18. M. George, L. Wiklund, M. Aastrup, J. Pousette, B. Thunholm, T. Saldeen, L. Wernroth, B. Zaren and L. Holmberg,*Eur J Clin Invest.*, 2001, **31**, 1083-94.
19. C. Kross, *J. Prevent. Med.*, 2002, **10**, 3–10.
20. A. Cockburn, C. W. Heppner and J. L. C. M. Dorne. *Encyclopedia of Food Safety*, 2014,**2,** 332-336.
21. WHO: World Health Organization, Guidelines for Drinking-water Quality, 4th edition, 2011,http://apps.who.int/iris/bitstream/10665/44584/1/9789241548151_eng.pdf.
22. S. Jagtap, M. K. Yenkie, N. Labhsetwar and S. Rayalu, *Chem. Rev.*, 2012**, 112,**2454–2466.
23. S. Ayoob, A. K. Gupta, T. Venugopal and A. Bhat, A., *Environ. Sci.Technol.*, 2008, **38,**401–470.
24. M. Mohapatra, S. Anand, B. K. Mishra, D. E. Giles and P. Singh, *J. Environ. Manage.*, 2009, **91**, 67–77.
25. A. Bhatnagar and M. Sillanpaa. *Chem. Eng. J.*,2011, **168**, 493-504.
26. M. Bandpi, D. J. Elliott and M. A. Zazouli, *J. Environ. Health Sci. Eng.*, 2013, **11**, 35.
27. S. P. Suriyaraj, T. Vijayaraghavan, P. Biji and R. Selvakumar, *J.Environ.Chem.Eng.*,2014, **2**, 444-454.
28. A. Bhatnagar, E. Kumar and M. Sillanpa, *Chem. Eng. J.*, 2011, **171**, 811–840.
29. P. Loganathan, S. Vigneswaran, J. Kandasamy and R. Naidu,*J. Hazard. Mater.*,2013, **248**, 1-19.
30. V. Tomar and D. Kumar, *Chem. Central J.*, 2013, **7**, 1–15.
31. M. G. Sujana, H. K. Pradhan and S. Anand, *J Hazard Mater.*, 2008, **16**, 120–125.
32. P. Loganathan, S. Vigneswaranand J. Kandasamy, *J. Environ. Manage.*,2013,**131**, 363-374
33. P. Loganathan, S. Vigneswaran and J. Kandasamy,*J Environ Manage.*, 2013, **15**, 363-74.

34. A. Omowunmi, Sadik, N. Du, I. Yazgan and V. Okello, Nanotechnology Applications for Clean Water (Second Edition), 2014, 95-108.
35. M. M. Khin, A. S. Nair, V. JagadeeshBabu, R. Murugan and S. Ramakrishna, *Energy Environ. Sci.*, 2012, **5**, 8075-8109.
36. T. Pradeepand Anshup, *Thin Solid Films*, 2009,**517**, 6441–6478.
37. M. T. M. Pendergast and M. V. Eric, Hoek,*Energy Environ. Sci.*, 2011, **4**, 1946-1971.
38. S. Kar and P. K. Tewari, *A volume in Woodhead Publishing Series in Civil and Structural Engineering*, 2013, 364–427.
39. X. Qu, J. J. Pedro, Alvarez and Q. Li. *Water Res.*,2013, **47**, 3931–3946.
40. T. Pradeep and M. S. Bootharaju. *Water Recla.Sustain.*, 2014, 317-342.
41. R. R. Devi, I. M. Umlong and P. K. Raul, *J. Exp. Nanosci.*,2014, **9**, 512-524.
42. S. M. Maliyekkal, A. K. Sharma and L. Philip,*Water Res.*, 2006, **40**, 3497–3506.
43. E. Kumar, A. Bhatnagar, U. Kumar and M. Sillanpaa, *J Hazard Mater.*, 2011, **186,**1042–1049.
44. P. K. Raul, R. R. Devi, I. M. Umlong, S. Banerjee, L. Singh and M. Purkait, *J. Nanosci. Nanotechnol.*, 2012, **12**, 3922–3930.
45. K. S. Prasad, Y. Amin and K. Selvaraj,*J Hazard Mater.*, 2014, **276**, 232-40.
46. T. Zhang, Q. Li, Z. Mei, H. Xiao, H. Lu and Y. Zhou, *Desalination and Water Treat.*, 2013, **52**, 16-18.
47. T. Zhang, Q. Li, H. Xiao, Z. Mei, H. Lu and Y. Zhou,*Appl. Clay Sci.*,2013, **72**, 117–123.
48. K. Biswas, S. Debnath and U. C. Ghosh, *Sep. Sci. Technol.*,2010, **45**, 472-485.
49. S. Deng, H. Liu, W. Zhou, J. Huang and G. Yu, *J Hazard Mater.*, 2011, **186**, 1360-1366.
50. A. Ghosh, S. Chakrabarti, K. Biswas and U. C Ghosh, *Appl. Surf. Sci.*,2014, **307**, 665–676.
51. M. Mohapatra, T. Padhi, S. Anand and B. K. Mishra, *Desalination and Water Treat.*, 2012, **50**, 376-386.
52. L. Li, D. Xu, X. Li, W. Liu and Y. Jia, *New J. Chem.*,2014, **38**, 5445-5452.
53. Thakre, S. Rayalu, R. Kawade, S. Meshram, J. Subrt and N. Labhsetwar, *J Hazard Mater.*, 2010, **180**, 122–130.
54. Z. Li, S. Deng, X. Zhang, W. Zhou, J. Huang and G. Yu, *Frontiers of Environ. Sci. Eng. China*, 2010, **4**, 414-420.
55. S. Chidambaram, S. Manikandan, A. L. Ramanathan, M. V. Prasanna, C. Thivya, U. Karmegam, R. Thilagavathi and K. Rajkumar, *Appl Water Sci.*, 2013, **3**, 741–751.
56. Chai, Y. Wang, N. Zhao, W. Yang and X. You, *Water Res.*, 2013, **1**, 4040-4049.
57. L. Chen, B.Y. He, S. He, T. J. Wang, C. L. Su and Y. Jin, *Powder Technol.*, 2012, **227**, 3–8.
58. Zhang, Chang, Chen, Lin, Wang, Ting-Jie, Su, Chao-Li, Jin and Yong,*Appl. Surf. Sci.*,**317**, 552-559.
59. M. Poursaberi, K. Hassanisadi, K. Torkestani and M. Zare,*ChemEng J.*, 2012 **189**, 117–125.
60. N. Minju, K. V. Swaroop, K. Haribabu, V. Sivasubramanian and P. Senthil Kumar, *Desalination* and *WaterTreat.*, 2013, 1-10.
61. X. Zhao, J. Wang, F. Wu, T. Wang, Y. Cai, Y. Shi and G. Jiang, *J Hazard Mater.*, 2010, **173**, 102-109.
62. M. Bhaumik, T. Y. Leswifi, A. Maity, V. V. Srinivasu and M. S. Onyango,*J Hazard Mater.*, 2011, **186**, 150-159.
63. C. Gao, X. Yu, T. Luo, Y. Jia, B. Sun, J. Liu and X. Huang, *J. Mater. Chem. A,* 2014, **2**, 2119-2128.
64. N. Thakur, S. A. Kumar, H. Parab, A. K. Pandey, P. Bhatt, S. D. Kumar and A. V. R. Reddy, *RSC Adv.*,2014, **4**, 10350-10357.
65. V. Kumar, N. Talreja, D. Deva, N. Sankararamakrishnan, A. Sharma and N. Verma,*Desalination*, 2011, **282**, 27–38.
66. A. Mahapatra, B. G. Mishra, and G. Hota, *Ind. Eng. Chem. Res.*, 2013, **52**, 1554–1561.
67. B. Y. Lee, K. Behler, M. E. Kurtoglu, Meghan, A. Wynosky-Dolfi, R. F. Rest and Y. Gogotsi, *J Nanopart Res.*, 2010, **12**, 2511–2519.
68. S.P.Suriyaraj, Mamatha M. Pillai, Amitava Bhatacharya and R.Selvakumar, *RSC Adv.*, 2015 **5**, 68420–68429
69. N. Viswanathan and S. Meenakshi, *Colloids Surf.,B: Biointerfaces*, 2009, **72**, 88–93.
70. C. Jing, J. Cui, Y. Huang, and A. Li,*ACS Appl. Mater. Interfaces*, 2012, **4**, 714–720.
71. A. K. Gupta, D. Deva , A. Sharma and N. Verma, *Ind. Eng. Chem. Res.*, 2009, **48**, 9697–9707.
72. Y. Ma, S. Wang, M. Fan, W. Gong and B. Gao, *J Hazard Mater.*, 2009, **168**, 1140–1146.
73. Janardhana, C. Rao, G. N. Sathish, R. Saikumar, P. Sunilkumar, V.Anil madhav and M. Vijay, *Indian J. Chem. Technol.*,2007, **14**, 350-354.
74. H. Jin, Z. Ji, J. Yuan, J. Li, M. Liu, C. Xu, J. Dong, P. Hou and S. Hou. *J. Alloys Compd.*,2015, **620**, 361-367.
75. Y. Li , S. Wang, X. Zhang, J. Wei, C. Xu, Z. Luan and D. Wu, *Mater. Res. Bull.*,2003, **38**,469–476.
76. N. Chen N, Z. Y. Zhang, C. P. Feng, N. Sugiura N, M. Li and R. Z. Chen, *J Colloid Interface Sci.*, 2010a, **348**, 579–584.
77. N. Chen, Z. Y. Zhang, C. P. Feng, N. Sugiura, M. Li, R. Z. Chen and D. R. Zhu, *J Hazard Mater.*, 2010b, **183**, 460–465.
78. S. Sundaram, N. Viswanathan and S. Meenakshi, *J Hazard Mater.*, 2008,**155**, 206–215.
79. G. E. Poinern, M. K. Ghosh Y. J. Ng, T. B. Issa, S. Anand and P. Singh,*J Hazard Mater.*, 2011, **185**, 29-37.
80. Zhang, H. Luo, L. Zheng, K. Wang, H. Li, Y. Wang and H. Feng, *J Hazard Mater.*, 2012, **241**, 418–426.
81. K. Pandi and N. Viswanathan, *Carbohydr. Polym.*,2014, **112**, 662-667.
82. S. Sundaram, N. Viswanathan and S. Meenakshi, *Biores. Technol.*, 2008,**99**, 8226–8230.
83. X. Yu, S. Tong, M. Ge and J. Zuo, *Carbohydr. Polym.*,2013,**92**, 269–275.
84. Y. Nie, C. Hu and C. Kong, *J Hazard Mater.*, 2012,**233**, 194–199.
85. S. M. Prabhu and S. Meenakshi,*Powder Technol.*,2014, **268**, 306–315.

86. S. G. Wang, Y. Ma, Y.-J. Shi and W.-X. Gong, *J. Chem. Technol. Biotechnol.*, 2009, **84**, 1043–1050.
87. M. Mohapatra, K. Rout, S. K. Gupta, P. Singh, S. Anand and B. K. Mishra, *J. Nanopart. Res.*, 2010, **12**, 681–686.
88. Wang, W. Xu, L. Chen, Y. Jia, L. Wang, X-J Huang, and J. Liu, *Chem. Eng. J.*, 2013, **231**, 198–205
89. S. Deng, H. Liu, W. Zhou, J. Huang and G. Yua,*J. Hazard. Mater.*,2011, **186**, 1360–1366.
90. X. Zhao , L. Zhang , P. Xiong , M. Wenjing, N. Qian and W. Lu, *Microporous Mesoporous Mater.*,2015, **201**, 91–98
91. Zhang, L. Chen, T. Wang, C. Su and Y. Jin,*Appl. Surf. Sci.*,2014, **317**, 552–559.
92. L. Chen, H-X. Wu, T. Wang, Y. Jin, Y. Zhang and X. Dou, *Powder Technol.*,2009, **193**, 59–64.
93. M. Vithanage, A. U. Rajapaksh, M. S. Bootharaju and T. Pradeep, *Colloids Surf., B:Physicochem. Eng.* Aspects, 2014, **462**, 124–130.
94. W. Wei, X. Wang, Y. Wang, M. Xu, J. Cui and Z. Wei, *Desalination and Water Treat.*,2014, **52**, 6219-6229.
95. Yang, L. Gao, Y. Wang, X. Tian and S. Komarneni, *MicroporousMesoporous Mater.*,2014, **197**,156–163.
96. Lin Chen, Bo-Yang He, Shuai He, Ting-Jie Wang, Chao-Li Su and Yong Jin, *Powder Technol.*, 2012,**227**, 3–8.
97. N. Chen, C. Feng and M. Li, *Clean Techn Environ Policy*, 2013.
98. A. Goswami and M. K. Purkait, *J. Water Process Eng*, 2014, **1**, 91–100.
99. Q. Shi, Y. Huangb and C. Jing, *J. Mater. Chem. A,* 2013,**1**, 12797-12803.
100. L. Lv, J. He, M. Wei, D. G. Evans and X. Duan, *J. Hazard. Mater.*,*B,* 2006, **133**, 119–128.
101. J. Nouri, R. Nabizadeh, M. J. rad, M. Yunesian and F. Moattar, *Desalination and Water Treat.*, 2014, **52**, 4369-4375.
102. S. K. Swain, T. Patnaik and R. K. Dey, *Desalination and.Water Treat.*, 2013,**51**, 4368-4378.
103. P. Koilraj, S. Kannan, *Chem. Eng. J.*, 2013, **234**, 406–415.
104. S.K. Swain, Tanushree Patnaik, P.C. Patnaik, UshaJha and R.K. Dey, *Chem. Eng. J*, 2013, **215,** 763-771
105. S. Gao, R. Sun, Z. Wei, H. Zhao, H. Y., Li and F. Hu*J. Fluorine Chem.*,2009, **130**, 550–556.
106. X. Yu, S. Ton, M. Ge and J. Zuo, *Carbohydr. Polym.*,2013, **92**, 269– 275.
107. T. Zhang, Q. Li, H. Xiao, H. Lu, H. and Y. Zhou, *Ind. Eng. Chem. Res.*, 2012, **51**, 11490-11498.
108. T. Wu, L. Mao and H. Wang, *RSC Adv.*, 2015, **5**, 23246- 23254
109. M. Ansari, M. Kazemipour, M. Dehghani, and M. Kazemipour, *J. Fluorine Chem.*,2011, **132**, 516-520.
110. S. S. Ramamurthy, Y. Chen, M. K. Kalyan, G. N. Rao, J. Chelli and S. Mitra, *J. Nanosci. Nanotechnol.*, 2011, 11, 3552-3559.
111. Y. H. Li, S. Wang, X. Zhang, J. Wei, C. Xu, Z. Luan, D. Wu and B. Wei, *Environ. Technol.*, 2003, **24**, 391-398.
112. N. Sankararamakrishnan, N. Singha and A. Gupta, *RSC Adv.*, 2013, **3**, 22421-9
113. Y. Chen, Q. Zhang, L. Chen, H. Bai and L. Li, *J. Mater. Chem. A,* 2013, **1**, 13101-13110.
114. H. Golestanifar, A. Asadi, A. Alinezhad, B. Haybati & M. Vosoughi, *Desalination and Water Treat.*, 2015, 1-8
115. H. Demiral and G. Gündüzoğlu, *Bioresour Technol.*, 2010, **101**, 1675-80.
116. A. Bhatnagar, E. Kumar and M. Sillanpaa,*Chem. Eng. J.*, 2010, **163**, 317–323.
117. M. Zhang, B. Gao, Y. Yao, Y. Xue and M. Inyang, *Chem. Eng. J.*,2012, **210**, 26–32.
118. R. Saad, S. Hamoudi and K. Belkacemi, *J. Porous Mater.*,2008, **15**, 315-323.
119. H. Jiang, P. Chen, S. Luo, X. Tu, Q. Cao and M. Shu, *Appl. Surf. Sci.*,2013, **284**, 942–949.
120. Motamedi, M. T. Atoueiand M. Z. Kassaee, *Mater. Res. Bull.*, 2014, **54**, 34–40.
121. T. Wang, J. Lin, Z. Chen, M. Megharaj and R. Naidu, *J. Clean. Prod.*, 2014, **83**, 413–419.
122. Mikami, Y. Sakamoto, Y. Yoshinaga and T. Okuhara*Appl. Catal., B: Environmental*, 2003, **44**,79–86.
123. M. A. Tofighy and T. Mohammadi, *Chem. Eng. Res. Des.* 2012, **90**, 1815–1822.
124. A. Khani and M. Mirzaei, 2nd International IUPAC Conference on Green Chemistry, 14-19 September 2008, Russia.
125. R. Mukherjee and S. De, *J. Membr. Sci.*,2014, **466**, 281–292.
126. M. A. Khan, Y. Ahn, M. Kumar, W. Lee, B. Min, G. Kim, D. Cho, W. Park and B. Jeon,*Sep. Sci. Technol.*,2011, **46**, 2575-2584.
127. A. Halajnia, S. Oustan, N. Najafi, A. R. Khataee and A. Lakzian, *Appl. Clay Sci.*,2012, **70**, 28–36.
128. S. Tezuka, R. Chitrakar, A. Sonoda, K. Ooi and T. Tomida, *Adsorption*, 2005, **11**, 751-755.
129. S. Chatterjee and S. H. Woo, *J. Hazard. Mater.*,2009, **164**, 1012–1018.
130. E. Eroglu V. Agarwa, M. Bradshaw, X. Chen, S. M. Smith, C. L. Raston and K. SwaminathanIyer, *Green Chem.*, 2012, **14**, 2682-2685.
131. T. Yang, K. Doudrickand P. Westerhoff,*Water Res.*, 2013, **47**, 1299-307.
132. S. Park, H. J. Kim, J. S. Kim, K. Yoo, J. C. Lee, W. A. Anderson and J. H. Lee, *J NanosciNanotechnol.*, 2007, **7**, 4069-72.
133. H. Kato and A. Kudo, *Phys. Chem. Chem. Phys.*,2002b, **4**, 2833
134. A. Devadas, S. Vasudevan and F. Epron*J. Hazard. Mater.*,2011, **185**, 1412-1417.
135. Y. N. Guo, J. H. Cheng, Y. Y. Hu and D. Li, *Appl. Catal., B:Environmental*, 2012, **125**, 21-27.
136. Z. Xu, L. Chen, Y. Shao, D. Yin and S. Zheng, *Ind. Eng. Chem. Res.*, 2009, **48**, 8356–8363.
137. O. Hamanoi and A. Kudo,*Chemistry Letters*, 2002, **31**, 838-839.
138. T. Sato, K. I. Sato, Y. Fujishiro, T. Yoshioka and A. Okuwaki, *J. Chem. Technol. Biotechnol.*,1996, **67**, 345-349.
139. Y. Liu, S. Li , Z. Chen and M. Megharaj , R. Naidu, *Chemosphere* 2014, **108**, 426-432.
140. A. O. Ibhadon and P. Fitzpatrick,*Catal.*, 2013, **3**, 189-218.
141. B. Ayati, A. Ahmadpour, F. Bamoharram, B. Tanhaei, M. Manttari and M. Sillanpaa, *Chemosphere*, 2014, **107**, 163-174.

142. U. I. GayaaandA. H. Abdullah. *Photochem. Photobiol., C:Photochemistry Reviews*,2008, **9**, 1–12.
143. S. Emad, S. Elmolla and M. Chaudhuri, *Desalination*, 2010, **252**, 46–52.
144. M. N. Chong, B. Jin, C. W. K. Chow and C. Saint, *Water Res.*,2010, **44**, 2997–3027.
145. J. Zhang, P. Zhou, J. Liub and J. Yu *Phys.Chem.Chem.Phys.*, 2014, **16**, 20382.
146. S. D. Mo and W. Y. Ching, *Phys Rev B Condens Matter.*, 1995, **51**, 13023-13032.
147. T. Luttrell, S. Halpegamage and J. Tao, 2014, *Sci Rep.* **4**, 1-8
148. A. Fujishima, T. N. Rao and D. A. Tryk, *J. Photochem. Photobiol., C:Photochemistry Reviews*, 2000, **1**, 1–21
149. Z. Yigit and H. Inan, *Water Air Soil Pollut: Focus*, 2009, **9**, 237 – 243.
150. Z. Luo, A. S. Poyraz, C. H. Kuo, R. Miao, Y. Meng, S. Y. Chen, T. Jiang, C. Wenos, and S. L. Suib, *Chem. Mater.*, 2015, **27**, 6–17.
151. A. D. Paola, M. Bellardita and L. P. Brookite, *Catal.*, 2013, **3**, 36-73.
152. D. C. Hurum, A. G. Agrios and K. A. Gray,*J. Phys. Chem. B*, 2003, **107**, 4545–4549.
153. J. Sa, T. Berger, K. Fottinger, A. Riss, J. A. Anderson and H. Vinek, *J. Catal.*,2005, **234**, 282–291.
154. N. Wehbe, M. Jaafar, C. Guillard, J. M. Herrmann, S. Miachon, E. Puzenat and N. Guilhaume, *Appl. Catal., A:General*, 2009, **368**, 1–8.
155. R. Jin, W. Gao, J. Chen, H. Zeng, F. Zhang, Z. Liu and N. Guan, *J. Photochem. Photobiol., A:Chemistry*, 2004, **162**, 585–590.
156. K. T. Ranjit, T. K. Varadarajan and B. Viswanathan, *J. Photochem. Photobiol.,A:Chemistry*, 1995, **89**, 67–68.
157. K. Kobwittaya and S. Sirivithayapakorn, *J.SaudiChem Soc.*, 2014, **18**, 291–298.
158. J. Sa, C. A. Aguera, S. Gross and J. A. Anderson, *Appl. Catal., B: Environmental*, 2009, **85**, 192–200.
159. F. Zhang, R. Jin, J. Chen, C. Shao, W. Gao, L. Li and N. Guan, *J. Catal.*, 2005, **232**, 2424–431.
160. M. Shand and J. A. Anderson, *Catal. Sci. Technol.*, 2013, **3**, 879-899.
161. M. C. Raphu, J. McPherson, E. van der Lingen, J. A. Anderson and M. S. Scurrell, *Gold Bulletin*, 2010, **43**, 334-334.
162. J. A. Anderson, *Catal. Today*, 2011, **175**, 316-321.
163. J. A. Anderson, *Catal. Today*, 2012, **181**, 171–176.
164. S. Rengaraj and X. Z. Li, *Chemosphere*, 2007, **66**, 5930–5938.
165. A. V. Lozovskii, I. V. Stolyarova, R. V. Prikhod and V. V. Goncharuk, *J. Water Chem. Technol.*, 2009, **31**, 360–366.
166. K. Doudrick, O. Monzon, A. Mangonon, K. Hristovski and P. Westerhoff,*ASCE J. Environ. Eng.*, 2012, **138**, 852–861.
167. J. Hsu, C. Liao and Y. Wei, *Sustain. Environ. Res.*, 2011, **21**, 353-359.
168. A. Su and R. W. Puls, *Environ. Sci. Technol.*, 2004, **38**, 2715-2720.
169. S.Ziajahromi, M. Khanizadeh, M. Khiadani, A. D. Zand and M. Mehrdad, *Middle East J Sci Res.*,2013, **16**, 205-209.
170. C. Yang and H. L. Lee,*Water Res.*, 2005, **39**, 884-894.
171. Y. Zhang, Y. Li, J. Li, L. Hu and X. Zheng, *Chem. Eng. J.*,2011, **171**, 526-531.
172. S. Choe, Y. Chang, K. Hwang and J. Khim, *Chemosphere*, 2000, **41**, 1307-1311.
173. C.Yang and H. L. Lee,*Water Res.*, 2005, **39**, 884-94.
174. W. Wang, Z. Jin , T. Li, H. Zhang and S. Gao, *Chemosphere*, 2006, **65**,1396–1404.
175. N. Krasae, K. Wantala, P. Tantriratna and N. Grisdanurak, *Appl. Environ. Res.*,2014, **36**, 15-23.
176. Y. H. Liou, C. J. Lin, S. C. Weng, H. H. Ou and S. L. Lo, *Environ. Sci. Technol.*, 2009, 43, 2482-2488.
177. J. R. Pan, C. Huang, W. P. Hsieh and B. J. Wu, *Sep. Purif.Technol,*. 2012, **84**, 52 –55.
178. Q. Shi, Y. Huang and C. Jing, *J. Mater. Chem. A,* 2013, **1**, 12797-12803.
179. X. Cai, Y. Gao Q. Sun, Z. Chen, M. Megharaj and R. Naidu, *Chem. Eng. J.*,2014, **244**, 19-26.
180. A. Ensie and S. Samad, *Desalination*, 2014, **347**, 1–9.
181. B.Su and R. W. Puls, *Environ. Sci. Technol.*, 2004, **38**, 2715-2720.
182. S. Xu and D. D. Sun, *Int. J. Hydrogen Energy*, 2009, **34**,6096–6104.
183. Qian, Z. Zhao, J. C. Velazquez, L. A. Pretzer, K. N. Hecka and M. S. Wong, *RSC, Nanoscale*, 2014, **6**, 358.
184. S. Jung, S. Bae and W. Le, *Environ Sci Technol.*, 2014, **48**, 9651-8.
185. S. Ambonguilat, H. Gallard, A. Garron, F. Epron and J. P. Croue, *Water Res.*,2006, **40**, 675-682.
186. Z. Gao, Y. Zhang, D. Li, C. J. Werth, Y. Zhang and X.Zhou, *J Hazard Mater.*, 2015, **3**, 425-431.
187. M. S. Kim,S. H. Chung,C. J. Yoo,M. S. Lee,I. H. Choand D.W. Lee, *Appl. Catal., B: Environmental*, 2013, **142**, 354-361.
188. Witońska, S. Karski and J. Gołuchowska, *Kinet. Catal.*,2007, **48**, 823-828.
189. F. Deganello, L. F. Liotta, A. Macaluso, A. M. Venezia and G. Deganello, *Appl. Catal., B: Environmental*,2000, **24**, 265–273.
190. A. Roveda, A. Benedetti, F. Pinna and G. Strukul, *InorganicaChimicaActa*, 2003, **349**, 203–208.
191. R. M. Mohameda and E.S. Baeissa, *J.Ind.Eng. Chem.*, 2014, **20**, 1367–1372.
192. Tawfik A. Saleh (2013). The Role of Carbon Nanotubes in Enhancement of Photocatalysis, Synthesis and applications of Carbon Nanotubes and their composites, Dr. Satoru Suzuki (Ed.), ISBN: 978-953-51-1125-2, InTech, DOI: 10.5772/51050.
193. J. Yu, T. Ma, G. Liu and B. Cheng, *Dalton Trans.*, 2011,**40**, 6635-6644.
194. L. Zhang, Y. Wang, T. Xu, S. Zhu and Y. Zhu, *J. Mol. Catal. A: Chem.*,2010, **331**, 7–14.
195. Z. D. Meng, L. Zhu, S. Ye , Q. Sun, K. Ullah, K. Y. Cho and W.C. Oh, *Nanoscale Res. Lett.*, 2013, **8**, 189.

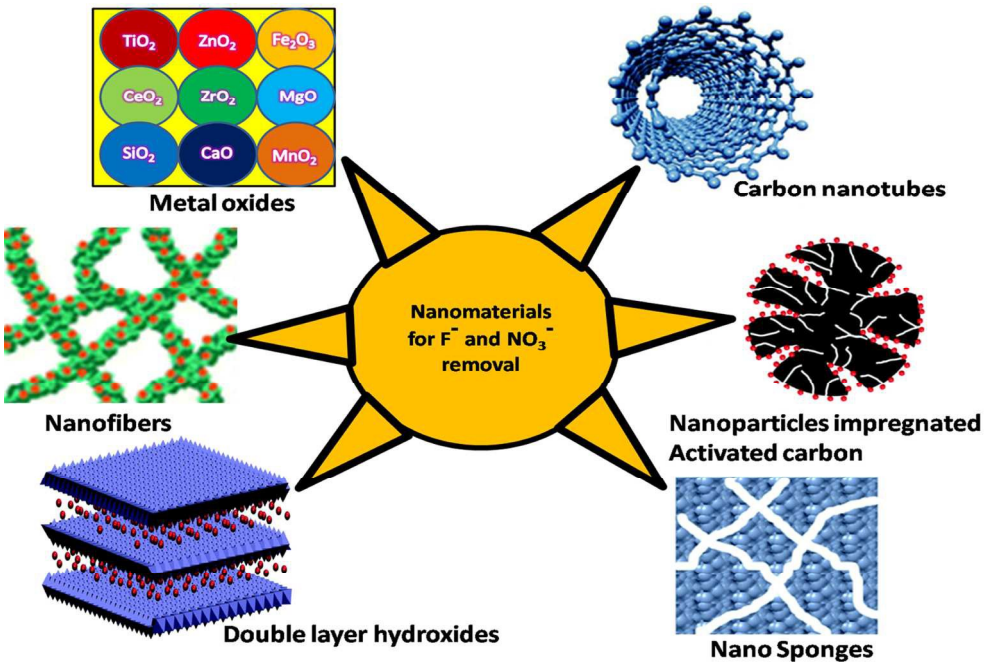

150x99mm (300 x 300 DPI)